UiT The Arctic University of Norway

Faculty of Science and Technology
Department of Physics and Technology

Polar Mesospheric Winter Echoes - an analysis of selected cases

Kristine Ettestad

FYS-3931 Master's Thesis in Space Physics
31 May 2022

Abstract

Polar Mesospheric Winter Echoes (PMWE) are strong coherent radar echoes, from the upper mesosphere at 55-85 km that are observed typically from end of August until beginning of May. Some models to explain PMWE formation suggest that they form because of turbulence in the atmosphere. Other models suggest that the PMWEs form like summer polar mesospheric echoes (PMSE) where charged dust particles must be present in addition to the turbulence. To examine the validity of the models, this work considered the PMWE detections made between 2008 and 2020 with the EISCAT VHF 224 MHz radar. PMWE were found in 11 datasets. Analyses of the PMWE spectra showed that they are better described with a Gauss profile rather than a Lorentz profile; the amplitudes, widths and frequency shifts of the spectra were derived and presented as function of time and altitude. These values were not vastly different from those of the PMSE that was considered for comparison. In 8 of the PMWE observations, the EISCAT heater was also operated; the heater emits HF radio waves that instantaneously raise the electron temperature at the altitude where the radio wave is attenuated. It was found that PMWE observed without heating had a larger overall spectral width than those observed with heating. The heater is operated in on-off modes, and it was noted that two of the PMWE observations during heating showed signal overshoot when the heater was turned off again. Such overshoots are commonly observed in PMSE and attributed to the effects of charged dust. The author concludes that the overshoot observation indicates that these two PMWEs most likely also form in the presence of charged dust. For the other PMWE observations it is unclear whether the pure turbulence assumption or the dust turbulence model applies. Python codes were written for data evaluation, which can be found in the appendix of the work.

’Just relax, but stay focused.’

-Lakshmi Narayanan Viswanathan 2022

Acknowledgements

I would like to thank my supervisor Ingrid Mann and co-supervisors Lakshmi Narayanan Viswanathan and Tinna Gunnarsdottir for supporting me, helping me stay calm, and always taking the time to answer questions. I always looked forward to our weekly meetings. I would also like to thank my partner and fellow master student Aleksander Johan Henriksen, this journey would not have been the same without you. Lastly I would like to thank my family and friends for keeping me grounded and always checking in on me.

Contents

List of Figures

List of Tables

Abbreviations

ALWIN	Alomar Wind radar
CET	Central European Time
EED	Equivalent Electron Density
FWHM	Full Width at Half Maximum
MAARSY	Middle Atmospheric Alomar Radars System
MLT	Mesosphere - Lower Thermosphere
MSPs	Meteoric Smoke Particles
PMSE	Polar Mesospheric Summer Echoes
PMWE	Polar Mesospheric Winter Echoes
RTG	Real Time Graph
TAR	Tape ARchive
TRO	Tromsø
VHF	Very High Frequency

1 Introduction

40 years ago, the first reported observation of strong coherent radar echoes, from upper mesospheric region at high northern latitude during summer months, in Very High Frequency (VHF) range took place[20]. Later, these were noted to occur throughout the whole year although for different seasons and varying in strength. The echoes in the summer season were stronger in comparison to the echoes in winter[8]. The summer echoes were named Polar mesospheric Summer Echoes(PMSE) and the winter echoes Polar Mesospheric Winter Echoes(PMWE). PMSE typically occurs within the mesospheric altitude region 80-90 km. PMWE are found at a lower altitude range of 55-85 km mainly occurring from end of August until beginning of May. It was believed only occurring during the winter months, hence given its name indicating it being a winter phenomenon. On the other hand, recent observations have shown that it occurs all year round[10].

PMWE have been observed during high-energy electron precipitation, increased background levels during solar proton events and artificial heating of the ionosphere[8]. What makes PMWE interesting is the many theories as to why the echoes appear. One such theory proposed the echoes to occur due to breaking of gravity waves while another claim the occurrence to be due to neutral turbulence excited by wind shear[1]. In recent years observations done by EISCAT Scientific Association (EISCAT) VHF radar has made Strelnikov et al.(2021)[20] questioned if atmosphere turbulence alone can explain why we are able to observe PMWE, and has led to the inclusion of what is known as Mesospheric Smoke Particles(MSPs). MSPs is one of the main factors as

to why we observe PMSE, another important factors being the cold summer mesosphere creating MSP embedded ice and neutral atmosphere turbulence. The similarities between the two echoes has brought forth the question if the nature of the two phenomena could be similar. However during peak PMWE periods, being end of September until beginning of October and end of February until beginning of March[13], the mesosphere is warmer and ice particles are not found. Therefore PMWE could not be due to MSP embedded ice or ice alone like PMSE, leaving only the inclusion of charged MSP and neutral atmospheric turbulence. The two theories on the nature of PMWE focused on in this thesis will be dusty turbulence theory, which includes MSPs, and pure turbulence theory.

Overshooting is a phenomena that happens when PMSE is heated by an ionospheric heating facility operating in radio frequencies. When the heater is turned on PMSE becomes weaker, and when the heater is turned off the PMSE returns stronger than it was before the heater was turned on. The increase after the heater is turned off is due to the charging of the dusty ice or pure ice particles present in the coherent echo[7]. PMWE can also show overshoot characteristics but only if dust plays a role in the occurrence of the echo[5].

The main objective of this thesis is to use PMWE observations by EISCAT VHF radar to further look into what might be the nature of PMWE, using both artificial heated PMWE observations and observations without. The structure of the thesis has been set as following: Chapter 2 gives an overview and introduction to the physics of the atmosphere and specifically the mesosphere, then dust in mesosphere and polar mesospheric echoes. Sub chapter 2.3 presents EISCAT VHF radar and the EISCAT heating facility including the physics behind a phenomena connected to artificial heating called overshoot. Chapter 3 cover how data were obtain and unpacked in MATLAB for the days of PMWE observations, how a fitting were applied to the PMWE spectrum, processing of the data in Python and two types of noise in data. Chapter 4 presents interesting results separating PMWE observations without artificial heating and heated observations. PMWE is in sub chapter 4.3 compared to a PMSE observation. Chapter 5 conclude results from chapter 4 and discuss further work on the data.

2

Background

Chapter 2 starts in 2.1 with an introduction to earths atmosphere focusing on the mesosphere and dust found in the layer. Chapter 2.2 introduces the two coherent echoes found in the mesosphere being PMSE and PMWE presented accordingly. The next sub chapter, 2.3, covers EISCAT and discuss instruments used to measure the two coherent echoes, also presenting EISCAT heating facility and the physics behind a phenomena connected to artificial heating known as overshoot.

2.1 Earths atmosphere

Feeling the sun on your skin on a warm summer day or listening to the leaves rustling in the wind are all possible due to Earths atmosphere. The atmosphere is our planets protective blanket allowing life to exist on Earth. In addition to its critical role for life to exist it is also a place of great wonders for researchers, students or people taking the time to look up once in a while.

The atmosphere consists of 5 different layers, the four lowest ones are shown in figure 2.1, classified by vertical structure of temperature. The stratification of the layers is, in combination with energy input and output, due to a balance between gravity and pressure forces[3]. Pressure and temperature differences drive large scale circulations. The atmospheric waves and turbulence results in

the mixing of contents of the the 3 lower atmospheric layers.

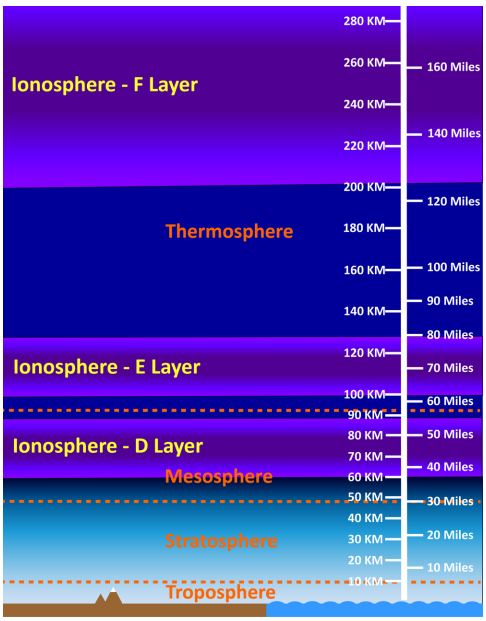

Figure 2.1: An illustration of the layers of the atmosphere and the ionospheric D-, E- and F-layer. The altitudes indicating the beginning and end of layers and atmospheric regions are approximate. Figure from: https://homapilot.com/articles/ionosphere/

The ionosphere is known as the region coexisting with the mesosphere and thermosphere, beginning at 60 km in the mesosphere and ending approximately at 1000 km in the exosphere(i.e. the uppermost layer in Earths atmosphere). It is defined as the region that is mainly ionized by solar radiation, and its name comes from the ionization of neutral species occurring in the region[19]. Like the atmosphere the ionosphere is also divided into layers called D-,E- and F-layer. D-region is the lowest layer found in the upper part of the mesosphere, E-region is the middle layer found in the thermosphere and the F-region is the uppermost layer found both in the thermosphere and exosphere. D-region has higher collisions due to denser coexisting mesosphere. During nighttime when the sun is not present, cosmic rays are the main source of ionization in this region. Their height and altitude span is not constant due to the size of the regions being dependent on input of radiation[19].

2.1.1 The mesosphere

The mesosphere starts at altitude ~50 km and ends at ~90 km. In this region we find the coldest temperatures in the atmosphere. Turbulence causes the gases to

mix, and it is the highest layer where mixing occurs effectively. The turbulence originates from lower part of the layer and altitudes. The mesosphere is a part of a region referred to as mesosphere - lower thermosphere(MLT). MLT spans over the altitude range 60-130 km. This region is dominated by effects from atmospheric waves such as gravity waves, planetary waves and tidal waves, all originating in the lower atmosphere[20]. Waves propagating upward from low altitudes grow exponentially due to decreasing atmospheric density.

Atmospheric gravity waves are an important factor to the mesospheric region circulation, since gravity waves can move vertically they can carry momentum and kinetic energy upward to higher altitudes. When reaching mesospheric altitudes a considerable amount of atmospheric gravity waves breaks and their momentum and energy is deposited[23]. In the mesosphere, breaking of gravity waves and residual circulation drives a polar flow circulation. In the summer season this circulation is directed towards equator. The summer circulation creates an upwelling of air, which due to an adiabatic expansion cools the air. This gives average temperatures of ~150 K, and can sink down to 100-130 K [11], well below the frost point of water ice. During winter when the flow direction changes, the polar regions experience adiabatic compression resulting in heating of the air. The two different flows result in an inverse temperature change, dependent on a polar- or equatorial flow.

2.1.2 Dust in mesosphere

There are three main dust types in the mesosphere. One is dust in the form of meteoric smoke, another being water ice in the polar summer and the third being a combination of the former two[14]. There is a daily input of meteoroids into earths atmosphere, ranging from 10-100 meteoric tons. Upon entering frictional heating takes place due to collisions with air molecules. The frictional heating gives enough energy to the meteoroids such that ablation takes place. Some of the ablated material is deposited at high altitudes in the atmosphere. This high altitude ablated meteoric material condenses and creates meteoric smoke particles. Some grow to a size of a 1-10 nm[5]. MSPs can bind to water due to its large dipole momentum, becoming a nuclei for condensation to take place in summer polar mesosphere, where temperature is below water frost point creating MSP embedded ice. This is the latter of the dust types, and will also only be referred to as dust.

2.2 Coherent radar echoes

2.2.1 PMSE

Dust can be found in the D-region plasma, existing in a charged state due to electrons collected onto the surface. As mentioned previously atmospheric gravity waves reaches mesospheric altitudes, and at the region where the D-layer plasma is found they grow unstable and turbulence arise[18]. Turbulence in combination with the charged dust creates spatial structures in the electron density that scatters radar signals in VHF range, giving strong echoes known as PMSE. The scattering comes from variation in the refractive index of the medium causing signal with a wavelength comparable to the spatial structure to be scattered. The spacing needed for efficient scattering to occur is called the Bragg scale. In mesospheric regions the Bragg scale is given as half the radar wavelength[15]. PMSE is visible for VHF radars operating in the frequency range ~50-900 MHz[17]. A closer look at PMSE is outside the scope of this thesis, however for further reading the paper by Markus Rapp and Lübken F.-J(2004)[14] should be considered.

2.2.2 PMWE

PMWE is like PMSE observed as an echo in the VHF range. In comparison to PMSE it is weaker and found at lower altitudes. It is observed in the altitude range 55-85 km. The echo was discovered occurring during the winter months and hence got its name as a winter echo. However it has been observed occurring all year round, even in summer when PMSE is present[13]. It was the Middle Atmospheric Alomar Radars System(MAARSY) at Andøya that in its first operating years 2011-2013 observed PMWE outside of winter season in the summer period of altitudes below 80 km. Before MAARSY the Alomar Wind radar(ALWIN) was used for observation of the echoes. Figure 2.2 shows the occurrence of PMWE throughout a whole year for both ALWIN and MAARSY. PMWE can be observed having two peak occurrence periods: end of September until beginning of October, and end of February until beginning of March. Although visible during summer the occurrence of the echo is low in comparison to the rest of the year. An extensive data analysis was performed by Latteck and Strelnikova[13] on the occurrence of PMWE using MAARSY at Andøya. Figure 2.3 is based on the observations from the two seasons 2011/2012 and 2013/2014. From the top panel showing seasonal variation of PMWE occurrence two peak periods can be observed being the same as mentioned previously.

An ongoing discussion on PMWE is what causes it to occur. One theory proposes scatter due to evanescent ion-acoustic waves (Kirkwood(2007)[8]), while Strel-

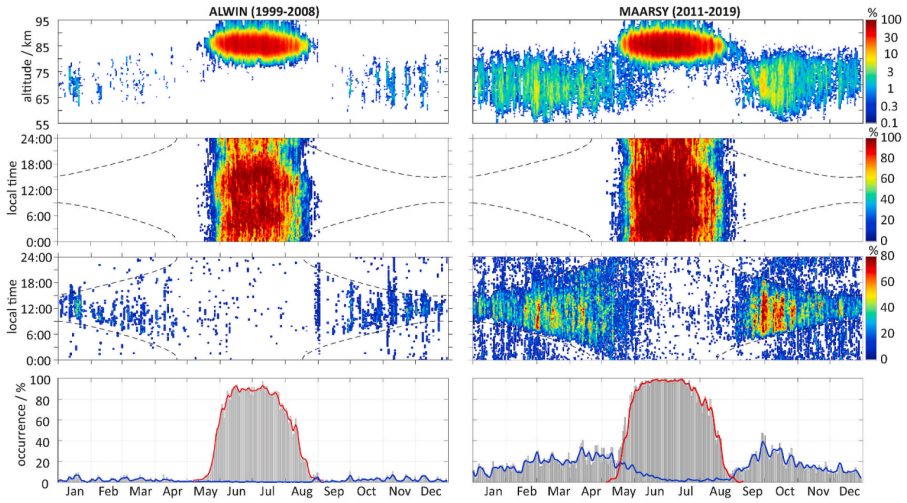

Figure 2.2: First row: occurrence rate for a whole year derived from radar volume reflectivities obtained by ALWIN and MAARSY. Second row: Seasonal and diurnal variations of PMSE. Third row: Seasonal and diurnal variations lower-altitude mesospheric echoes occurrence rate. Dashed black lines represents the solar zenith angle $\chi = 98°$. Fourth row: Seasonal variations of mesospheric echoes (grey area), lower-altitude mesospheric echoes (blue line) and PMSE (red line). Figure collected from paper by Latteck et al.(2021) [13]

nikov et al.(2021)[20] summarise a theory based on horizontal speed having velocities above 300 $\frac{m}{s}$. In this thesis, the two main theories focused on will be pure turbulent theory and dusty turbulent theory. The two theories are discussed further in the following section.

Pure turbulent theory suggest that PMWE comes from neutral air turbulence when background ionization is high enough[20]. It is important to note that this is suggested for PMWE found below ~85 km and above and including ~75 km. Dusty turbulent theory considers the winter mesosphere as 'contaminated' with MSPs in the form of charged aerosols of the order of 1 nm, creating a dusty plasma. EISCAT Scientific Association observed PMWE using its VHF radar. Only fine coherent structures at size of the Bragg scale will give an echo in the VHF range. In comparison to other MST radars such as MAARSY, the Bragg scale of EISCAT VHF radar is smaller(i.e 0.67 m) leading to the possibility of dust playing a role[20]. Strong neutral air turbulence alone should not yield a PMWE observation due to the formed structures are to be too diffuse, on the other hand including dust in the form of MSPs such small scale structure can form.

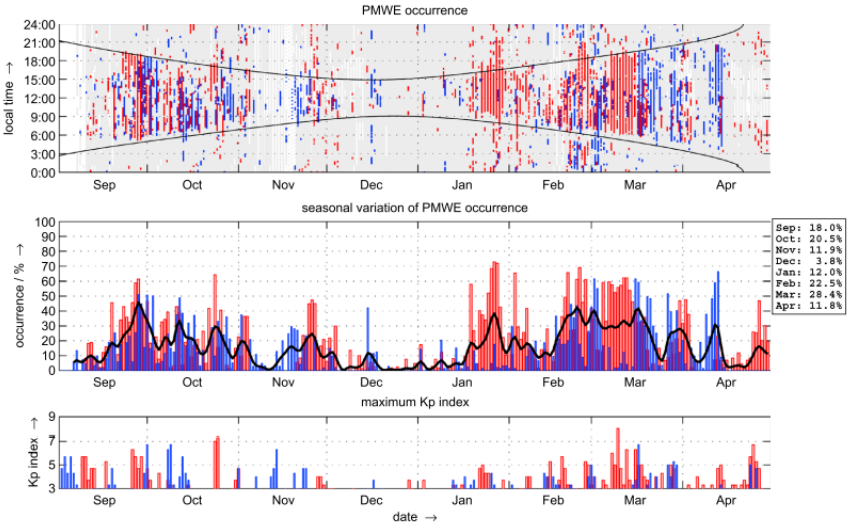

Figure 2.3: Seasonal variance of PMWE from September to April. The first plot shows PMWE occurrence for each month, the black line is the solar zenith angle. The second plot is occurrence rate in percentage of PMWE for each month. The last plot shows the kp indexes. Figure collected from paper by Latteck and Strelnikova(2015)[10]

A rocket project for investigating PMWE took place at Andøya Space Center in 2018 and was aimed to look into the nature of the echoes(Strelnikov et. al(2021)[20]). The conclusion of the campaign was that neither of the two present theories above could be excluded. One of the rockets proved that some PMWE was created by neutral air turbulence in combination with enhanced background ionization. It was also concluded from MSP measurements on-board the payload of two rockets that tiny dust particles($\leq$1 nm) are always present in the PMWE.

The focus of this thesis is to look closer at what might be the nature of PMWE. This will be done by looking trough archived data from EISCAT incoherent VHF radar for the years 2008-2020. The goal is to observe how these observations compare to Strelnikov's results focusing on the two PMWE origin theories. Other interesting benefits of the observations is getting an insight into the behaviour of the echo and maybe correlate some of it to PMSE. The next section will cover more on EISCAT and instruments used for observation of PMWE and PMSE, also discussing artificial heating and a phenomenon known as overshoot. The analysis of data from EISCAT VHF radar is discussed in detail in chapter 3.

2.3 EISCAT

2.3.1 EISCAT VHF radar

EISCAT VHF radar is placed in Ramfjordmoen close to Tromsø in northern Norway. It operates in the frequency band of 224 MHz and has a corresponding Bragg scale of 67 cm[25]. The radar can observe coherent echoes in altitude range 50-200 km using manda pulse code scheme. The frequency is high enough for small scale structures in the mesosphere to be observed and therefore making it especially good for detection of coherent scatter in the form of PMWE and PMSE. The EISCAT measurements are made with different radar codes having different sequences of radar pulses that determines the altitude resolution and altitude range of the observation. An often used code for observation of PMSE and PMWE is manda providing data from 50 to 200 km with a resolution of 0.18-0.36 km[24]. Other codes that cover the relevant altitudes are beata and arcd.

EISCAT VHF radar make data available trough the Madrigal database. The database stores and provide data from multiple EISCAT instruments and incoherent scatter radars placed all around the world. EISCAT VHF radar is preferable as an instrument since it operates in a different frequency compared to other radars such as MAARSY. A different frequency gives a different Bragg scale. Another important quality is that the radar also observes incoherent scatter at regions without PMSE/PMWE, due to this information on the ionosphere during the time of the PMSE/PMWE can be derived. The radar can also operate along with a heating facility, this is discussed further in the next section.

2.3.2 Heating

EISCAT VHF radar can operate simultaneous with artificial heating using the EISCAT Heating Facility. The heating facility consists of several antenna arrays that are located in Ramfjordmoen at the EISCAT site. It transmits radio waves at specific frequencies between 2.75-8 MHz[18] into the atmosphere. The low frequency radio waves interact with the ionosphere and increase the temperature of the electrons at different heights. The increase in electron temperature depends on factors such as the frequency of the transmitted waves and the electron contents. The radio waves can be modulated by changing power or polarization, and also by an on-off modulation. An on-off modulation is when the transmitters are turned on for a set amount of time(i.e. 90 s) and then off for a different amount of time or the same (i.e. 120 s).

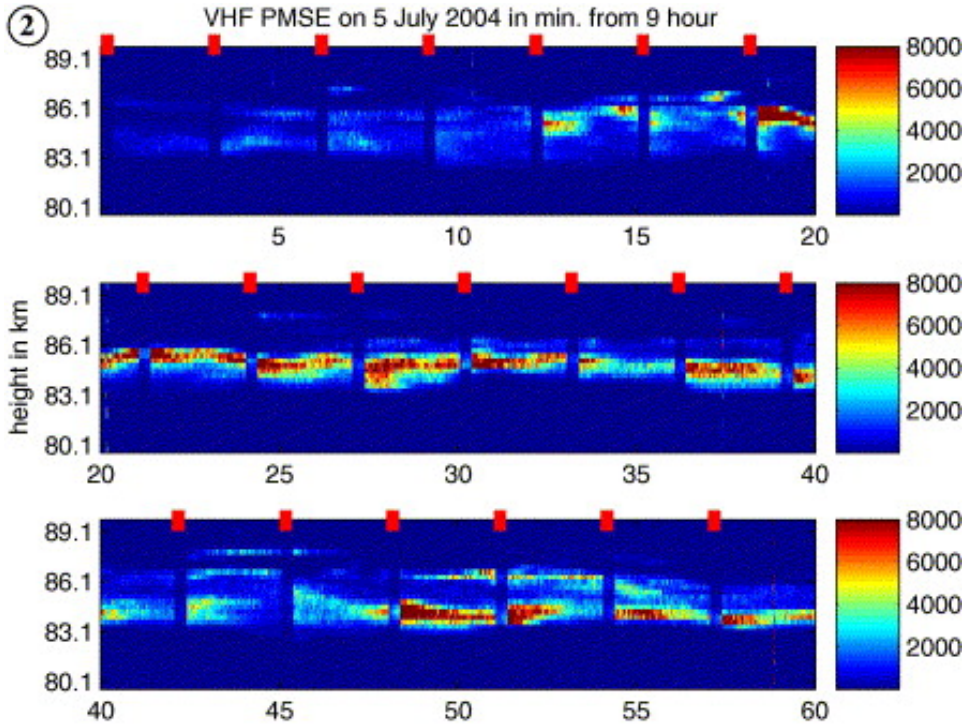

Figure 2.4: PMSE observations from 5 July 2004 with an overshoot heating cycle(20s on and 160s off heating), red lines indicate heating on. Colorbar shows intensity in an arbitrary scale. Figure collected from paper by O. Havnes et al.[4]

When heating is taking place at the same time as PMWE observations we can look for a pattern in the PMWE structure known as an overshoot effect. Overshoot occurs if dust particles are present at altitude and time of PMWE structures and also if the on-off modulation is within some certain values. The physics behind the process is as follows:
When the heater is turned on it will quickly increase the electron temperature and the influence of the dust particles onto the electrons weakens. The electron diffusivity is increased resulting in the electron density gradient becoming weaker, consequently not fully matching the Bragg scale condition. The heater must be on for up to 0.1 s for the electrons to heat up and weaken the influence from the dust particles[4]. The higher electron temperature increases the electron current escalating collisions between the electrons and dust particles. Turning the heater off causes the electrons to rapidly return to their initial state before heating. The dust particle retain its negative charges and pushes the electrons away, increasing the electron density gradient. During the span of 100-160 s the electrons completely cools of and the PMWE returns to its initial state[9].
The overshoot effect is an already well known phenomenon when looking

at PMSE, since charged MSPs embedded ice and charged ice particles are a driving factor in its appearance during the summer months. Figure 2.4 shows overshoot effect for PMSE observation on 5 July 2004. When heating is turned on the observed PMSE structure weakens and blend into the background. After the heater is turned on there is an observable increase in intensity.

3

Data analysis

Sub chapter 3.1 discuss how PMWE observations and modulation of artificial heated observations were obtained, presenting the observation and modulations with heating parameters in separate tables. Sub chapter 3.2 being the longest chapter walks trough how data were processed and distributions fitted to data, showing figures of important steps along the way. Close to the end of sub chapter 3.2 the removal of noise is discussed leading into the final sub chapter 3.3 where two types of noise found in data is presented and discussed.

3.1 PMWE observations

In preparations for the thesis all observations done by EISCAT VHF radar from 2008 until 2020 was looked trough, excluding the months May, June and July each year. All observations were found trough Madrigal database, choosing EISCAT VHF radar as instrument. The goal of the research was to collect PMWE observations and over a span of 13 years 11 such observations were found, and are presented in table 3.1.

An observations was counted as PMWE if it showed an enhancement in EED at altitude region 55-95 km within the period from August to April. The echo/power measured by the radar through incoherent scattering is proportional to the electron density. Because PMWE echoes result from coherent scattering from

Bragg scale structures, we refer to it as EED. Figure 3.1 show what is classified as a PMWE observations. In altitude range 55-60 km enhanced electron density structures can be observed at time 12:30-14:00 [UT]. The structures occur at different altitudes with different intensity, but below the edge of increased electron density found close to 80 km.

Table 3.1: Table showing PMWE observations from 2012-2019, using EISCAT VHF radar. Table also shows date, time and duration of observation.

Year	Date	Time [UT]	Duration [min]	Code	Heating
2012	24.01	13:40	5	Manda 24 & 60	Yes
	25.01	11:30	15	Manda 24	Yes
		13:00	10		
		13:30	15		
	28.02	08:55	75	Manda 24	Yes
		11:00	15		
2013	20.03	09:20	10	Manda 60	Yes
2014	20.02	10:00	20	Manda 24	Yes
	21.11	10:50	60	Manda 60	Yes
	24.11	09:30	25	Manda 24	Yes
2015	04.11	10:15	15	Manda 60	No
2016	09.12	12:30	5	Manda 60	No
2017	25.10	09:35	10	Manda 60	No
2019	01.03	12:45	15	Manda 60	No
		13:15	30		

Table 3.2: Days of PMWE observations where heating is done. Time of heating and modulation used is also shown

Year	Date	Time on and off [UT]	Description of Modulation	Polzn
2012	24.01	10:08:00-14:06:24	24s on, 64s off	X
	25.01	12:02:00-14:02.24	24s on, 96s off	O
	28.02	08:30:00-11:36:00	24s on, 96s off	X
2013	20.03	09:23:00-13:00:00	1s on, 1s off	X
2014	20.02	10:02:57-11:41:31	48s on, 144s off	X
	21.11	10:15:00-14:00:00	15ms on, 40.6ms off	O
	24.11	09:27:00-11:01:40	48s on, 120s off	O

Table 3.2 show the days of PMWE observation where artificial heating done by EISCAT Heating Facility was occurring simultaneously with PMWE observation. The modulation and days of artificial heating was collected by looking trough handwritten heating logs made by the heating facility from 2012 until 2014.

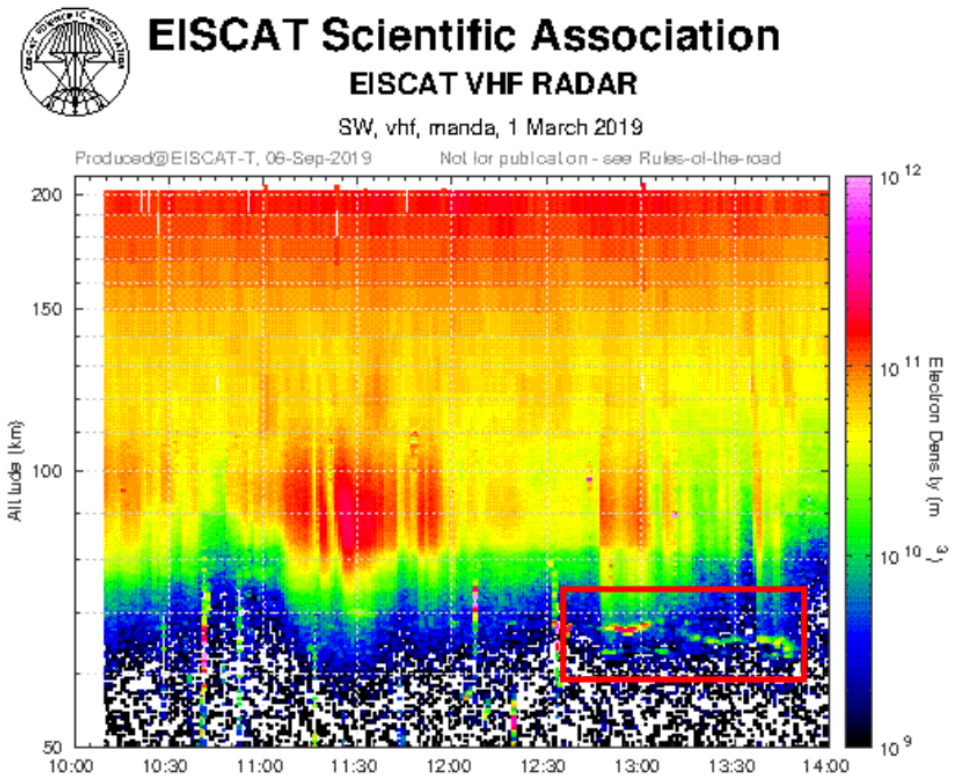

Figure 3.1: PMWE observation 1 March 2019. PMWE structure found inside red box

3.2 Fitting of data

Trough the EISCAT portal website (https://portal.eiscat.se/) data from observations performed by EISCAT radars can be collected, and were done for observations presented in table 3.1. The data is downloaded in a TAR-format. TAR stands for Tape ARchive and is commonly used to store multiple files in one single file. Within the TAR archive each of the data file in Matlab format is compressed to bzip2 format. To open a TAR-file and extract the data in MATLAB format an unzipping tool is needed. For data in this thesis 7-Zip was used, however PeaZip can also be used. After unzipping the files it was of interest to obtaining the Doppler spectrum of the PMWE. The routine used for obtaining the spectra is known as Real Time Graph(RTG) method (https://doi.org/10.5281/zenodo.4138625). The RTG method was run in MATLAB and an important input was sampling size in dumps. 1 dump corresponds to 4.8 s and for the artificial heated observations 1 dump were used, for the remaining non artificially heated observations 10 dumps (48 s) were used. The artificially heated observations were chosen to have a higher sampling rate to avoid aliasing, taking into account the small heating cycles ranging from 15 ms to 144 s.

The output from RTG method was unfitted data, such as spectral values, time and height, but the program also applied a Gaussian fit to the data and three spectral moments was given from it. To understand why the Gaussian fit was applied we should look at a plot of the PMWE Doppler Spectrum. The plot of the Doppler spectrum shown in figure 3.2 is for 9 December 2019, at time 12:35 and height 64.36 km. The time and height was found by looking for the highest echo-power-value in the PMWE structure, the plotting was done by using Python. Note the shape of the plot looking like a Gaussian distribution, also known as a normal distribution.

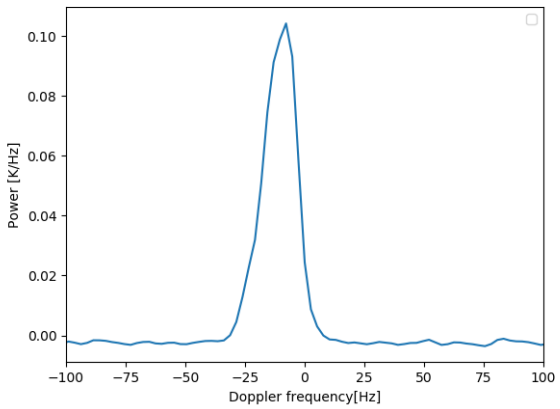

Figure 3.2: Plot of power over Doppler frequency for PMWE observed 9 December 2016. Plotted for time 12:35 [UT] and altitude 64.36 km

Although the shape looks to be like a Gaussian distribution, a Lorentzian distribution should also be considered. In the altitude region ~ 70-90 km where we find PMWE, incoherent scattering occurs from the highly damped ion-acoustic waves[21] [16] [22]. The shape of the incoherent scatter spectrum in the D-region is well represented by a Lorentzian distribution. PMSE structures gives a coherent scatter, and when detected by incoherent scatter radars the spectrum takes on the shape of a Gaussian distribution. Since PMWE like PMSE is coherent scatter, we can assume the same principles applies. It is generally accepted from theory of coherent scatter that its spectrum has a Gaussian shape, and is why we should predict the shape of figure 3.2 to be that of a Gaussian.

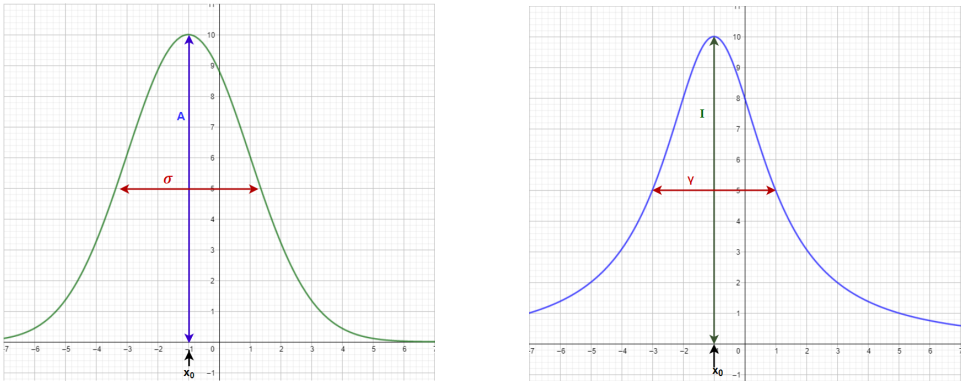

(a) Gaussian **(b)** Lorentzian

Figure 3.3: Gaussian and Lorentzian distributions illustrating parameters found in equation 3.1 and 3.2.

$$G(x) = Ae^{\frac{-(x-x_0)^2}{2\sigma^2}} \tag{3.1}$$

$$L(x) = \frac{I \cdot \gamma^2}{(x-x_0)^2 + \gamma^2} \tag{3.2}$$

The shape of the spectrum is important since a fit can be applied to the data. Without a fit it is challenging to compare days of observations in terms of not having parameters able to determine important features of the scatter spectrum. Applying a Gaussian or Lorentzian fit gives trivial information about spectrum like 'height of curve peak', 'Full Width at Half Maximum' referred to as 'width' and 'frequency at curve peak', illustrated in figure 3.3. With these parameters its easier to observe how the PMWE varies throughout its occurrence, how it varies for different cases and what is common throughout observations. 'height of curve peak', 'Full Width at Half Maximum' and 'frequency at curve peak' are the three spectral moments given by the RTG Gaussian fitting. We will get back to exactly how we utilize these parameters later in this sub chapter. For now we need to take a look at which of the two fits are best for the data, and lets start by looking at the features of the two distributions.

Gaussian and Lorentz distributions are both symmetric about their center points with relatively small 'tails' at its side, making most of the area found around and close to its curve peak[6]. When talking about the Gaussian distribution it is often characterised by its 'bell-shaped' distribution, whereas the Lorentz seems more narrower in comparison. The difference between the distributions is observed more clearly in their mathematical expression. Equation 3.1 is the

mathematical expression for the Gaussian function and equation 3.2 is for the Lorentz function. Figure 3.3 shows visually the parameters given in the equation. It is important to note that Full Width at Half Maximum(FWHM) of peak value is σ multiplied with $2\sqrt{2\ln 2} \approx 2.35482$, for simplification when later referring to values of σ the multiplication is taken into account but not mentioned.

Parameters for function 3.1:

A – Height of curve peak

$x0$ – Frequency at curve peak

$\sigma \cdot 2.35482$ – FWHM of peak value

Parameters for function 3.2:

I – Height of curve peak

$x0$ – Frequency at curve peak

γ – Width

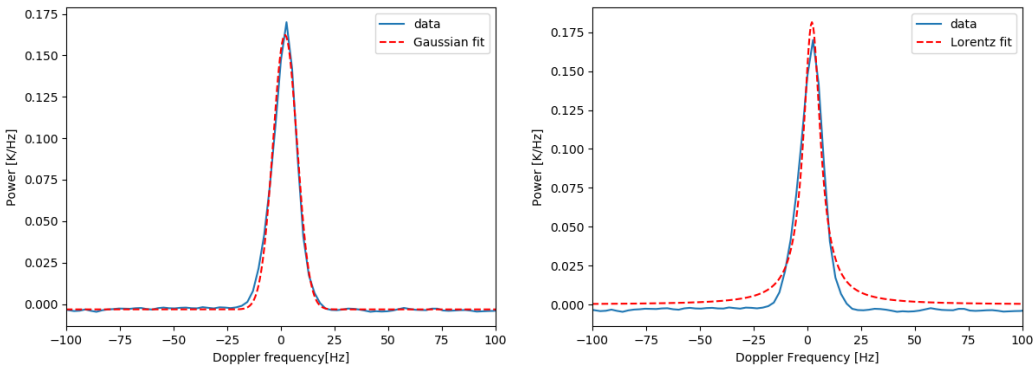

(a) Gaussian fitting **(b)** Lorentz fitting

Figure 3.4: PMWE spectrum showing Gaussian and Lorentz fitting onto the spectrum in figure 3.2.

In order to determine which of the two distributions would best fit our data both distributions were fitted and the corresponding function was plotted over the actual data. Although visual analysis can give a good overview of the fit and show to a degree if the fit is close to data, it is not precise enough for a conclusion. Therefore in addition to the visual representation the standard deviation errors on the parameters of the two fit were also collected from the

curve fitting algorithm used(i.e. curve fit from Scipy's optimize in Python). Figure 3.4 shows the Lorentz and the Gauss fitting, where 3.4a is the Gauss fitted and 3.4b is the Lorentz fitted.

Comparing the Gaussian and Lorentz fit from figure 3.4 we can already favor the Gaussian fit since the Lorentz fit looks to be deviating from data when Doppler frequencies are close to -20 Hz and 20 Hz. In addition the peak power of the fit 3.4b has a higher curve peak. As mentioned in the previous section a visually analysis is a good indicator when determine which fit to use, however to make an actual conclusion we should look to the standard deviation for the parameters collected from the algorithm used for the two fits:

Function 3.1:

$$A \approx 0.001012 \ \frac{\mathrm{K}}{\mathrm{Hz}}$$
$$x_0 \approx 0.03933 \text{ Hz}$$
$$\sigma \approx 0.03963 \text{ Hz}$$

Function 3.2:

$$I \approx 0.004059 \ \frac{\mathrm{K}}{\mathrm{Hz}}$$
$$x_0 \approx 0.1523 \text{ Hz}$$
$$\gamma \approx 0.1081 \text{ Hz}$$

When a distribution is fitted to a data the deviation of its parameters should be as low as possible to best describe the data, since lower values indicate the fit closely following the shape of the data.
Comparing the standard deviation of the 'height of curve peak' parameters I and A: I is close to 4 time higher when compared to A. It was earlier noted that the 'height of curve peak' for the Lorentzian fit seemed of higher value then the actual data and a standard deviation of $\sim 0.004 \ \frac{\mathrm{K}}{\mathrm{Hz}}$ in I reflects this. The lower standard deviation of $\sim 0.001 \ \frac{\mathrm{K}}{\mathrm{Hz}}$ in A shows that the Gaussian fit better represents the height of curve peak. Next we need to discuss the standard deviation in 'frequency at curve peak'. Both distributions use x_0 when describing frequency at curve peak and the standard deviation in the Lorentzian is ~ 4 times higher when compared to the Gaussian. Implying that the Gaussian fit better represents frequency at curve peak for the data. The last parameters is 'FWHM of peak value' and 'width'. Both parameters describes a feature related

to the width of the distribution. However it should be noted that in comparison to 'height of curve peak' and 'frequency at curve peak', where the parameters are describing the same height and frequency, these parameters are not describing the exact same width. γ has a standard deviation $\sim$3 times higher in comparison to the standard deviation of σ. It should come to no surprise that this again shows that the Gaussian fit better represents the width of the data. Based on the standard deviation of the Gaussian and Lorentzian parameters the Gaussian distribution was chosen as the best fit for the data.

Using RTG method in MATLAB a Gaussian fitting was applied to the unzipped files and the distribution parameters A, x_0 and σ was stored in separate folders. Opening the folder containing the parameters in Python each were used to create a contour plot showing all three parameters together with the same height and time interval as the PMWE structure. The name of the parameter from the Gaussian fitting was shortened when plotting and was renamed the following: height of curve peak is amplitude, FWHM of peak value is width and frequency at curve peak is shift. The contour plot used was Matplotlib's 'contourf' and in comparison to the packages other plot: 'contour' the former does not draw the polygon edges(i.e. the edges between different valued areas). This is how the three lower plots seen in figure 3.5 were created.

The top plot in figure 3.5 labeled 'EED' (acronym for equivalent electron density) was made by doing the following: Firstly accessing Madrigal Database (https://madrigal.eiscat.se/madrigal/single), selecting 'Incoherent Scatter Radars' under 'instrument category' and 'EISCAT Tromso VHF IS radar' under 'instrument'. Next 2014 was selected as year and November as month. After selecting both year and month a calendar appear showing days where the instrument was used and data is available by marking the area around the numbers as dark grey. Clicking on the date 24 the text 'Select experiment' appear and a list showing available experiments. The experiment containing 'manda@vhf' in its title was chosen. When selecting an experiment it is important to note that the date contained in the title of the experiment matches the date selected in the calendar and not from the day prior or after. After the experiment had been selected another text appeared: 'Select file'. There were mainly two different file types presented in the selection of files 'MAD6300' and 'MAD6400'. 'MAD6400' was chosen since it contained EED estimated using GUISDAP, whereas 'MAD6300' did not. Clicking the 'download file' button and choosing the option 'as is' the file was downloaded in a space-delimited ascii format. Inside the file each column represented a different parameter, however each column was separated by a different amount of spaces. The difference in spacing made it difficult to import the data into Python. The problem was in the unpacking program 'loadtxt' from the 'Numpy' module, used for importing data into Python. When using the program to import data a constant separation between the columns

Table 3.3: Amplitude threshold applied to PMWE observations.

Date	Threshold criteria [$\frac{K}{Hz}$]
24.01.2012	0.06
25.01.2012	0.03
28.02.2012	0.02
20.03.2013	0.01
20.04.2014	0.01
21.11.2014	0.01
24.11.2014	0.01
04.11.2015	0.01
09.12.2016	0.01
25.10.2017	0.01
01.02.2019	0.01

was needed. The problem was solved by opening the file in the text editing program 'Notepad++' and using the 'find an replace' command changing the uneven spacing between the columns to a single semicolon ';'. After editing the file it was opened in Python using 'loadtxt' and by setting the separating between the columns as ';'. The three values height, time and EED was extracted from the file in Python and the later plotted together with the two former parameters using the contour plot discussed in the previous section. The time and height interval was set to be the same as for the three other contour plots. The code for the programming done in Python when plotting the Gaussian moments and EED together can be found in appendix B.

The two lower subplots 'width' and 'shift' in figure 3.5 contains a dominating amount of noise, consequently making identifying values related to the PMWE structure challenging. In the paper by Narayanan et al.(2022)[12] a similar problem was discussed in terms of PMSE and the noise was removed by setting a threshold criteria of 0.01 $\frac{K}{Hz}$ on the amplitude, meaning only values above were identified as PMSE. Values found below the threshold value were set to Nan values. Nan stands for Not a number. The same method and threshold were applied to the Amplitude values in figure 3.5, changing values below 0.01 $\frac{K}{Hz}$ in Amplitude to Nan values, corresponding time an height in Width and shift was also changed to Nan values. The output of the threshold is shown in figure 3.6, where the white area around and outside the PMWE structures shows the Nan values. It can be noted from the figure that most of the noise found in 'width' and 'shift' in figure 3.5 has been removed and that only values related to the PMWE structure remain. For figures presented in this thesis showing Gaussian fitting outputs together with 'EED', similar to 3.6, the threshold applied to the amplitude for each observation is shown in table 3.3.

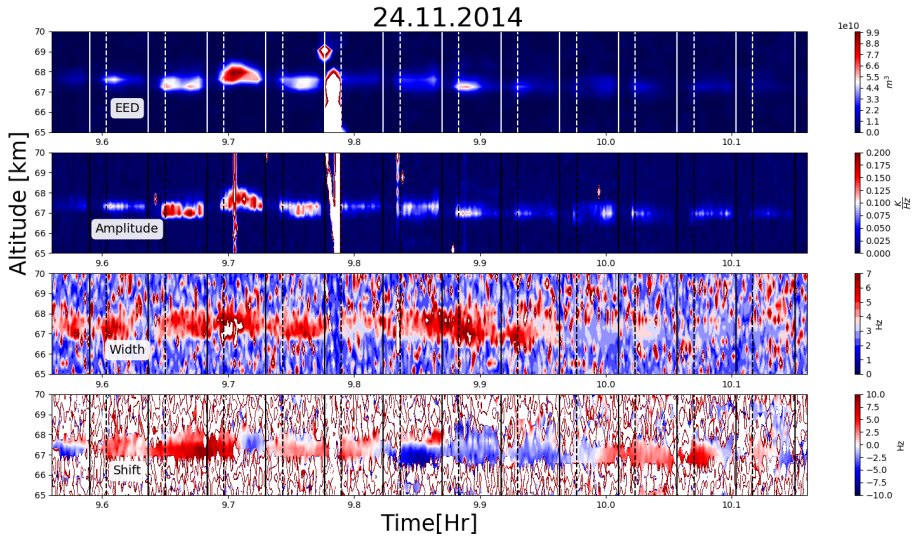

Figure 3.5: PMWE observation 24 November 2014. Time interval for all plots are 09:35-10:10 [UT]. The plots are from top to bottom EED (m^3), amplitude ($\frac{K}{Hz}$), width (Hz) and shift (Hz). The plots are presented without a noise removal threshold condition

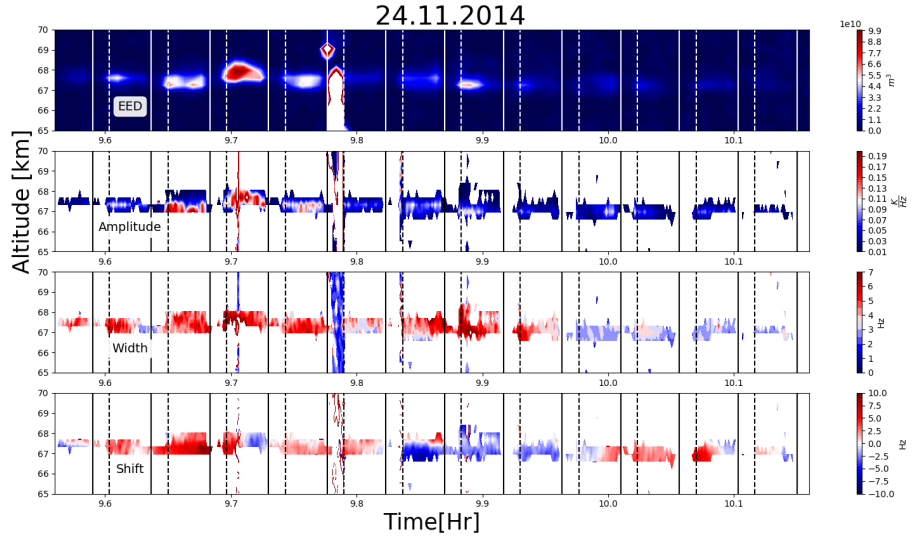

Figure 3.6: PMWE observation 24 November 2019. Time interval for all plots are 09:35-10:10 [UT]. The plots are from top to bottom EED (m^3), amplitude ($\frac{K}{Hz}$), width (Hz) and shift (Hz). A threshold condition of 0.01 $\frac{K}{Hz}$ has been applied to the amplitude and corresponding values in Width and shift.

The continuous white line in electron density and black line in Amplitude, Width and Shift indicates when artificial heating were taking place for figures 3.5 and 3.6. Dashed lines indicate when the artificial heating was turned off.

These lines were created using information of the artificial heating modulation found in table 3.2. The colour map chosen for plotting is named 'seismic' and were chosen due to the colors changing if the Doppler shift is positive (red) or negative (blue).

PMWE has been compared to physical traits of PMSE such as having a Gaussian distribution when plotting power over Doppler frequency and also when applying a noise threshold on the amplitude. Due to this, data from a PMSE observation from 10 July 2020 was collected and processed using the same steps as for the non artificial heated PMWE observation. The reason for doing this is to observe if our assumptions of the similarities are justified when comparing the behaviors of the two echoes. The resulting plots are found and discussed in sub chapter 4.3.

3.3 Noise

From figure 3.6 we observe before hour 9.8 and after 9.7 vertical lines appearing in all 4 plots. This is most likely noise caused by a disturbance or unwanted object in the radar beam while it was operating. This can happen if an illuminated target is within the radar beam causing unwanted scattering[25]. Noise can disrupt the data in such a way that information in the area where it appears is lost. For example in all 4 subplots in figure 3.6 the vertical noise found at time of heating before hour 9.8 is disruptive since it has hidden almost all information about the PMWE structure found within the same time interval. It is important to note that not all noise is the same. Some noise have high height of curve peak values when plotting the power over Doppler frequency and consequentially is included into data even when a threshold condition is applied[12]. The next two paragraphs will discuss this further.

There are two types of unwanted noise when discussing figures 3.5 and 3.6. The first one is noise found outside of the PMWE structure. When plotting the power over Doppler frequency for such area it has a wavy oscillating structure as shown in figure 3.7b. The Gaussian fitting of such structure has low height of curve peak values and are removed when applying a noise removal threshold condition.

The second unwanted noise is the vertical lines that was discussed in the beginning of this section. Figure 3.7a shows power over Doppler frequency for one of the maximum values found inside the vertical structure, at time 9.78 Hr and altitude 65.44 km. Such vertical noises often have high valued peak power at frequency far away from zero. When Gaussian fitting the 'height of curve peak' becomes the peak of the curve, even for frequency at peak value

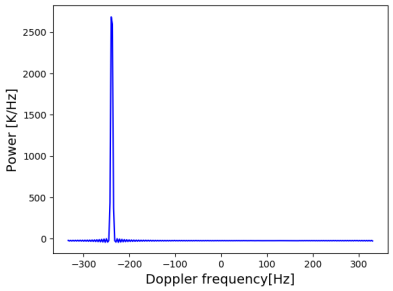

(a) PMWE spectrum at altitude 65.44 km and time 9.78 [Hr] for vertical noise observed in figures 3.5 and 3.6

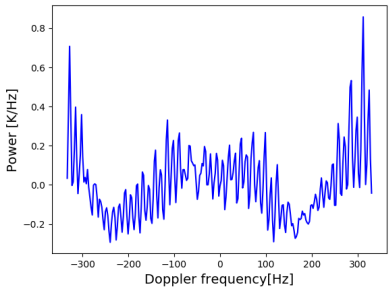

(b) PMWE spectrum at altitude 70.02 km and time 9.92 [Hr] for noise outside of PMWE structure

Figure 3.7: PMWE spectrum's for 24 November 2019 observation

found at high Doppler frequencies of hundreds of Hertz. The top of the curve observed in figure 3.7a has a power value of circa 2650 $\frac{K}{Hz}$, when in comparison to figure 3.6 strong PMWE has a value of 0.2 $\frac{K}{Hz}$. This is why such vertical structure noise is included into the data even when applying a noise removal threshold condition. A way to remove this noise could be to apply a threshold on Doppler frequencies as done for PMSE observations in the paper by Narayanan et al.(2022)[12].

4

Results and discussion

The following chapter will presents interesting results from the data analysis in chapter 3 and discuss the outputs. All outputs from chapter 3 can be found in appendix A. Chapter 4 starts in section 4.1 discussing the results of observations without artificial heating, followed by the artificially heated observations in sub chapter 4.2. 4.3 discuss similarities and differences between a PMSE observation and PMWE also discussing further work.

4.1 PMWE without heating

Figure 4.1 showing PMWE observation from 4 November 2015 has an interesting pattern found in its shift-values in time interval 10.3-10.5(10:18-10:30 [UT]) Shift changes rapidly between positive and negative Doppler velocities and during the same time period the width values are close to or above 7 Hz. Narayanan et al.(2022)[12] had similar behaviour showing in shift and width of a PMSE spectrum and it was discussed that such randomness in Doppler velocities is an indication for turbulence and the nature of the upward and downward velocity alterations could indicate the presence of Atmospheric gravity waves.

Another case where high values in Spectral width can be observed is in 4.2 in the time period ~12.55-12.60 (12:33-12:36 [UT]). The Spectral width has values

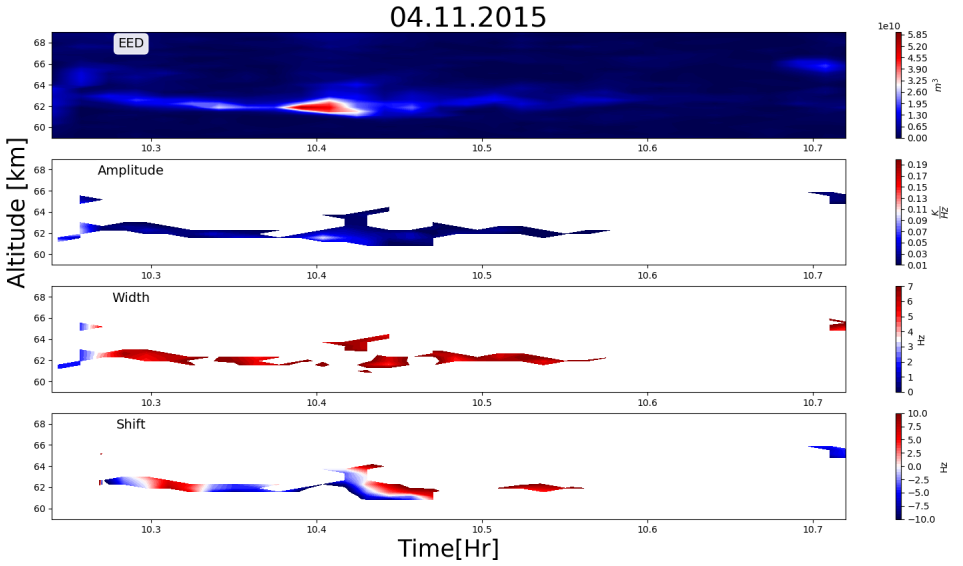

Figure 4.1: PMWE observation 4 November 2015. Time interval for all plots are 10:15-10:45 [UT]. The plots are from top to bottom EED (m^3), amplitude ($\frac{K}{Hz}$), width (Hz) and shift (Hz).

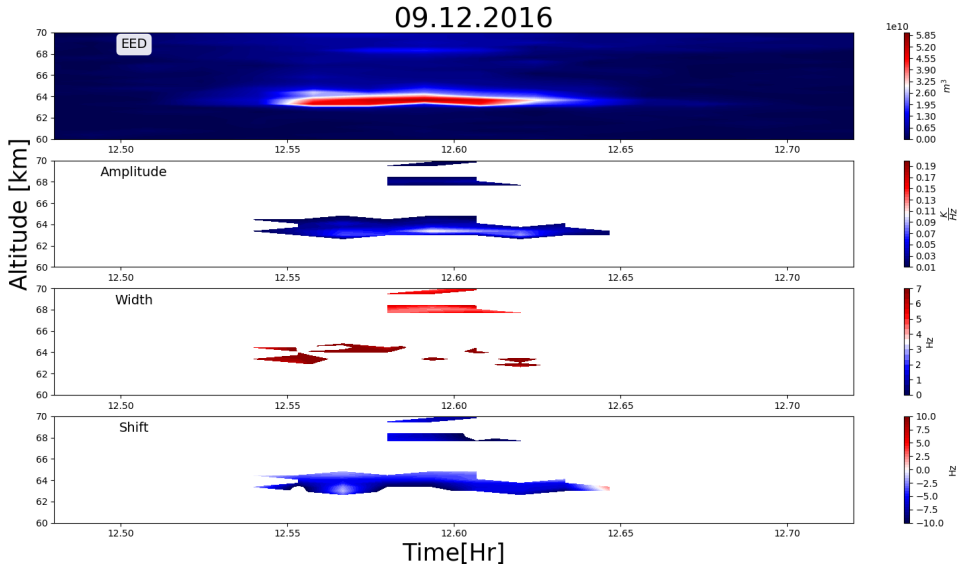

Figure 4.2: PMWE observation 9 December 2016. Time interval for all plots are 12:30-12:45 [UT]. The plots are from top to bottom EED (m^3), amplitude ($\frac{K}{Hz}$), width (Hz) and shift (Hz).

of or above 7 Hz, similar to figure 4.1, however there is no similar Doppler velocities fluctuations in the shift. It should be noted that the time of interest spans over a period of ~3 minutes for figure 4.2 whereas the previous case

was for 12 minutes. The time of observations is short and therefore should not be compared to the behaviour of the previous case which had a time interval being 4 times longer.

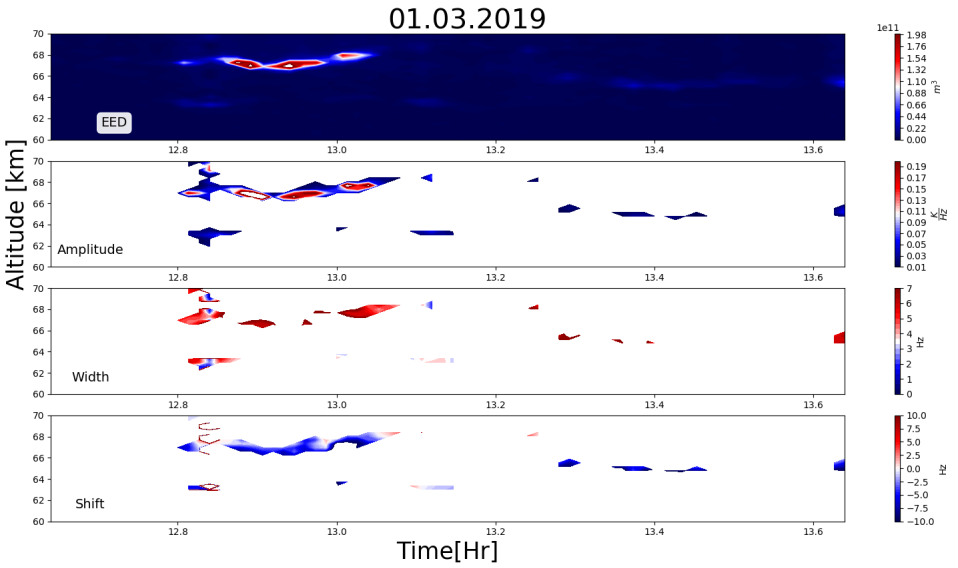

Figure 4.3: PMWE observation 1 March 2019. Time interval for all plots are 12:40-13:40 [UT]. The plots are from top to bottom EED (m^3), amplitude ($\frac{K}{Hz}$), width (Hz) and shift (Hz).

Figure 4.3 showing PMWE observed on 1 March 2019 has of all the non artificial heated observations the highest EED in the PMWE structure, the longest structure duration and its main structure found at an altitude of 66-70 km. The other 3 observations have electron densities of up to 1e10 m^3 in the PMWE structure, whereas this occurrence has values up to 1e11 m^3. This day of observation and the two previously discussed non artificial heated observations have on average a width of ~6 Hz at time of increased EED.

Kirkwood(2007)[8] presented a theory based on an earlier paper that an increase in width within PMWE structure indicated the presence of turbulence. However it was argued that the conclusion could not be made due to the measurements being taken with an antenna having a range resolution at 1 km. A reason for the wider spectra could simply be due to velocity shear coinciding with the PMWE. Therefore the widening of the PMWE spectrum is not enough to determine if the PMWE is from dusty turbulent or pure turbulent scattering.

4.2 PMWE with heating

24 November 2014 was out of all artificial heated observations the one having overshoot characteristics most similar to the PMSE overshoot seen in figure 2.4 in sub section 2.3. The PMWE overshoot observation is presented in figure 4.4.

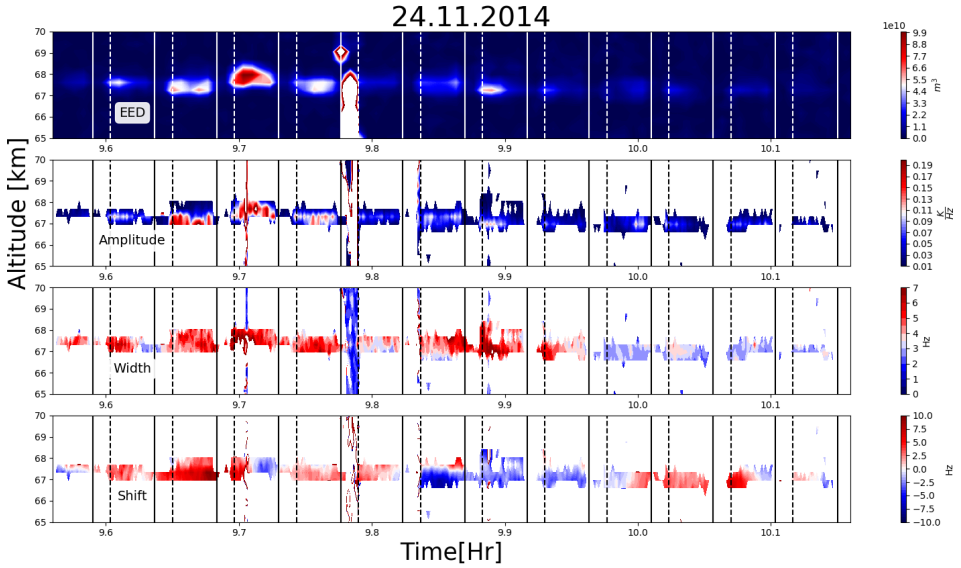

Figure 4.4: PMWE observation 24 November 2014. Time interval for all plots are 09:35-10:10 [UT]. The plots are from top to bottom EED (m^3), amplitude ($\frac{K}{Hz}$), width (Hz) and shift (Hz). Continuous white and black lines indicate when heating is turned on and dashed indicates when it was turned off.

When the heater is on the EED and amplitude in the two top panel of figure 4.4 decreases in value. Then when turning off the heater there can be observed an increase. This pattern is observed repeating but right before and after 10:00 weaker increases occur. This behavior is what is known as an overshoot effect(Kassa et al.(2005)[7], Havnes et al.(2001)[5]. The radar reflectivity is lowered because heating increases electron diffusivity and reduces the electron density gradient. Which is why during the on-time the echo strength is lowered. The increase after the heater is turned off is due to the negative charging of the dust particles pushing the electrons away. In doing so there arises a density gradient and increased PMWE strength. Without the presence of dust particles the PMWE would not have this behaviour. An explanation on why the overshooting effect is decreasing with increasing time might be due to the off time of the heating cycle. From table 3.2 we know the heating cycle for this day of observation: heating was on for 48 seconds and off for 120 seconds. The off time for the heating cycle may not be long enough to let the electrons cool completely. As shown by Biebricher et al.(2006)[2] this results

in the overshooting decreasing with increasing temperature. The dust particles charge grows with increasing temperature, because electrons collides more frequently, however this also results in plasma absorption becoming stronger. The latter dominates for higher temperatures and could explain why the EED and amplitude decreases at later times in figure 4.4. An off period of 160 seconds was recommended for cooling the electron gas enough.

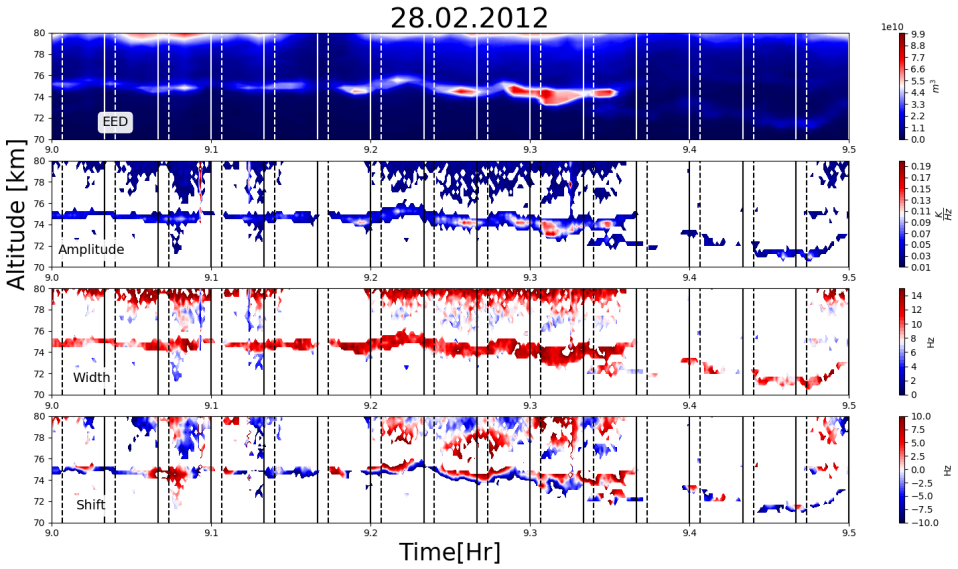

Figure 4.5: PMWE observation 28 February 2012. Time interval for all plots are 09:00-09:30 [UT]. The plots are from top to bottom EED (m^3), amplitude ($\frac{K}{Hz}$), width (Hz) and shift (Hz). Continuous white and black lines indicate when heating is turned on and dashed indicates when it was turned off.

Not every observation with artificial heating shows the same pattern as seen in figure 4.4. Looking at a PMWE observations from 28 February 2012 as seen in figure 4.5 we can note some differences. While heating is taking place the electron density does not reach as low values as observed in figure 4.4. After heating is turned off there is not as noticeable increase in density as seen previously. From the heating table 3.2 the on and off time of heating is 24 s on and 96 s off. Both are smaller than for 24 November 2014. As previously discussed a short off time does not allow electrons to cool enough and plasma absorption dominates, but why does the pattern of the PMWE look only slightly affected by the heating? Biebricher et al.(2006)[2] has one explanation for this, although related to PMSE. The overshoot effect is critically dependent on the amount of ionization occurring in the middle atmosphere at height of observation and below. If there is high solar activity the transmitted power by the heater is absorbed before reaching the altitude of PMSE. To strengthen this as a cause for the different behaviour to heating we should take a look at the EED plot

for both these days found in figure 4.13.

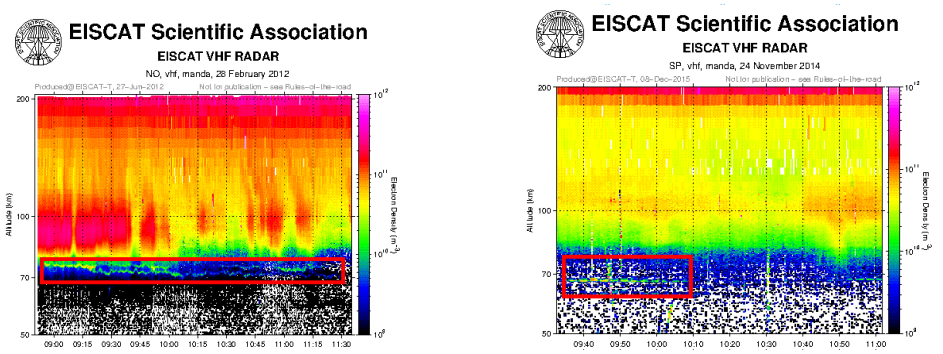

(a) PMWE observations 28 February 2012

(b) PMWE observation 24 November 2014

Figure 4.6: PMWE observations 28 February 2012 and 20 February 2014, PMWE structures can be observed inside the red boxes.

The PMWE occurred at higher altitudes where the electron densities were also higher on 28 February 2012. On 24 November 2014, the PMWE occurred at lower altitudes with less electron density. The higher electron density found above and around the PMWE structure on 28 February could potentially absorb heating before it reaches the PMWE and might be the reason why the PMWE is not as affected by heating.

It is important to note that even if the overshoot effect for the 28 February 2012 observation were not as distinct compared to 21 November 2014, the overshoot characteristics is still there indicating the presence of dust and its role in the occurrence. For the two artificial heated PMWE observations 24 November 2014 and 28 February 2012 overshoot characteristics could be observed during heating. This prove that dust played a role in the occurrence of both echoes supporting the dusty turbulence theory.

Not every artificial heating case is of interest due to observations where the heating modulation off-time is short. We can discuss this further using the PMWE observation from 20 March 2013 as an example. Heating modulation for this observation was 1 second on 1 second off. As discussed previously in this chapter the off-time is not long enough to let the electrons cool and return to its former state, before artificial heating took place. However we should also look into the on-time of the artificial heating modulation. The electron current negatively charging the dust particles does so most effectively after ~ 10 seconds[4]. With 1 second of artificial heating the amount of negative charges on the surface of dust particles should be really small. Without enough negative charges the electron density structure consequently arising when heating is

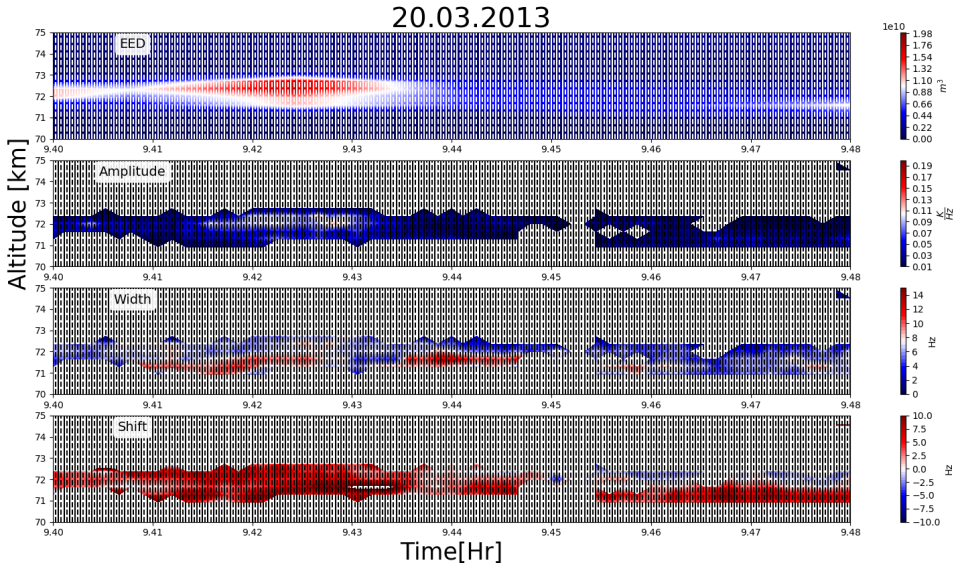

Figure 4.7: PMWE observation for 20 March 2013. Time interval for all plots are 09:25-09:30 [UT]. 09:25-09:30[UT]. The plots are from top to bottom EED (m^3), amplitude ($\frac{K}{Hz}$), width (Hz) and shift (Hz). Continuous white and black lines indicate when heating is turned on and dashed indicates when it was turned off.

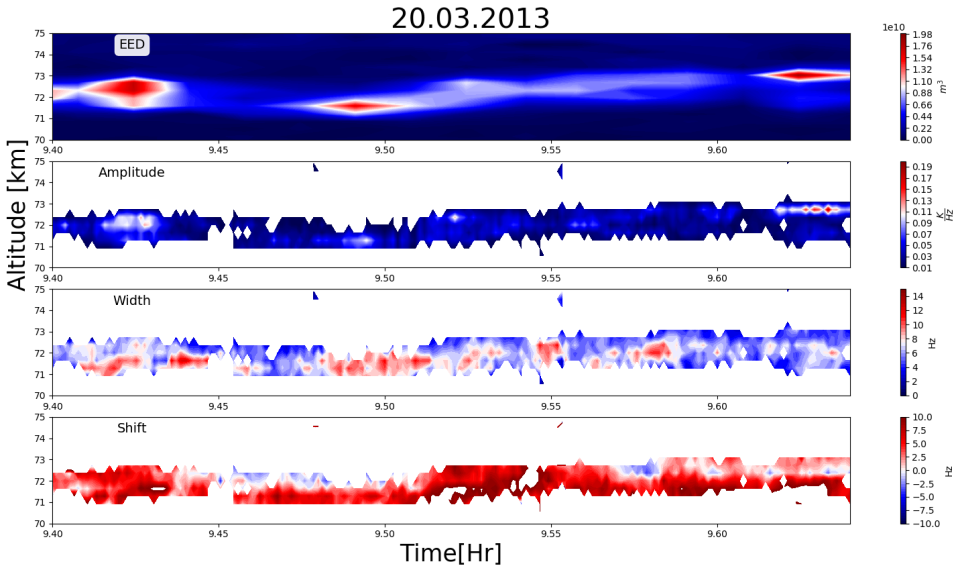

Figure 4.8: PMWE observation for 20 March 2013. Time interval for all plots are 09:25-09:40 [UT]. The plots are from top to bottom EED (m^3), amplitude ($\frac{K}{Hz}$), width (Hz) and shift (Hz).

turned off is diffuse and cant create a strong overshoot effect. Given both a too

short on- and of-time modulation we can expect the PMWE observation from that day, found in figure 4.7, to show no overshoot effect. Since figure 4.7 has heating on-off lines that mostly dominates the plot, an extra figure of the same PMWE observations without heating lines and for a longer time span can be found in figure 4.8. There is no rapid decreases or increases in electron density in figure 4.8. In comparison to what we observed in figure 4.7 the PMWE seems unaffected by the heating. If overshooting were to occur ignoring the short on- and of-time modulation then we would have expected the enhanced EED structure to be mostly made up by thin vertical lines, making the PMWE structure look like a bar code.

Having looked at three different PMWE observations with artificial heating and based on the papers by Kassa et al.(2005)[7] and Havnes et al.(2001)[5] an artificial heating modulation of ~20 second on-time and above or close to ~100 seconds off-time is preferable when looking for an overshoot effect. Excluding observations that has been discussed the two days of observation 25 January 2012 and 20 February 2014 have preferable artificial heating modulation, and will be looked into next.

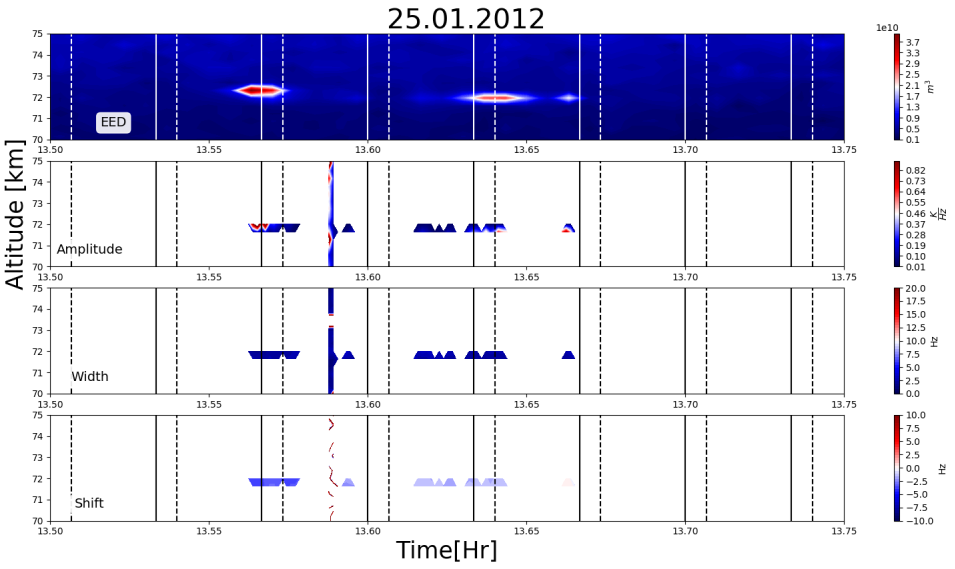

Figure 4.9: PMWE observation 25 January 2012. Time interval for all plots are 13:30-13:45 [UT]. The plots are from top to bottom EED (m^3), amplitude ($\frac{K}{Hz}$), width (Hz) and shift (Hz). Continuous white and black lines indicate when heating is turned on and dashed indicates when it was turned off.

For PMWE observation on 25 January 2012 the artificial heating modulation was 24 seconds on and 96 second off. From figure 4.9 showing the observation we can note that there is no overshoot effect in the enhanced EED structure

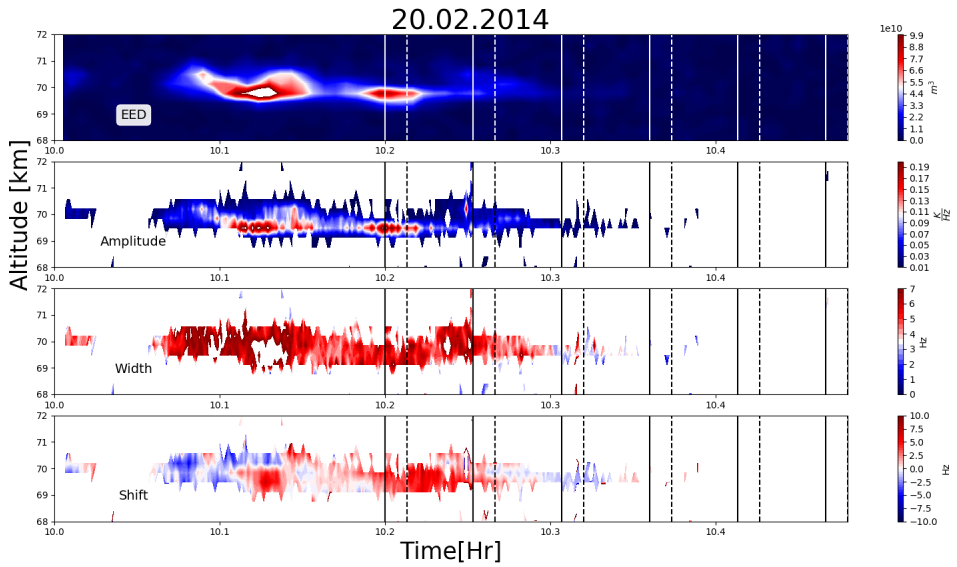

Figure 4.10: PMWE observation 20 February 2014. Time interval for all plots are 10:00-10:30 [UT]. The plots are from top to bottom EED (m^3), amplitude ($\frac{K}{Hz}$), width (Hz) and shift (Hz). Continuous white and black lines indicate when heating is turned on and dashed indicates when it was turned off.

after the heater is turned off.

The PMWE observation on 20 February 2014, seen in figure 4.10 had an artificial heating modulation of 48 seconds on and 144 second off. From the handwritten heating logs containing information of the modulation there was issues with heating for this day. As a consequence no precise artificial heating on and off lines could be illustrated before hour 10.2(10:12 [UT]), being a region of interest. Due to the uncertainties in artificial heating for the observation no overshoot effect will be discussed based on the observation.

When discussing dust in mesosphere it is important to know that there is no observational data on dust in this altitude range at all times, and precisely how dust varies in time and space is unknown. A consequence of this is that it cant be known if a PMWE observation is occurring when there is a large or small amount of dust present, or the exact size of dust. Overshoot is dependent on charging and charging interactions which would dependent on the size and amount of the dust particles[7]. Surprisingly artificial heated PMSE observations does not always show an overshoot effect[7], being a echo known to occur due to dust in combination with turbulence. Consequently no linear relation can be made between absent overshoot characteristic in artificial heated PMWE observations and the role of dust in forming the observed PMWE. For the

PMWE observation on 25 January 2012 no overshoot characteristics could be observed in the PMWE structure. As discussed this neither confirms or denies the role of dust in forming the observed PMWE. It should also not be excluded that the echo could arise from turbulence alone. It is quite possible that both pure turbulence and dusty turbulence theories are applicable for PMWE.

4.3 Comparison with PMSE

In section 3.4 we assumed that PMWE would follow the same principles as PMSE due to both echoes being coherent and therefore have a Gaussian distributed Doppler spectrum. By analysing a day of PMSE we can look at the similarities and differences and conclude if this assumption is justified or not. The day of PMSE was chosen to be 10 July 2020. A plot of electron density for this day is seen in figure 4.11

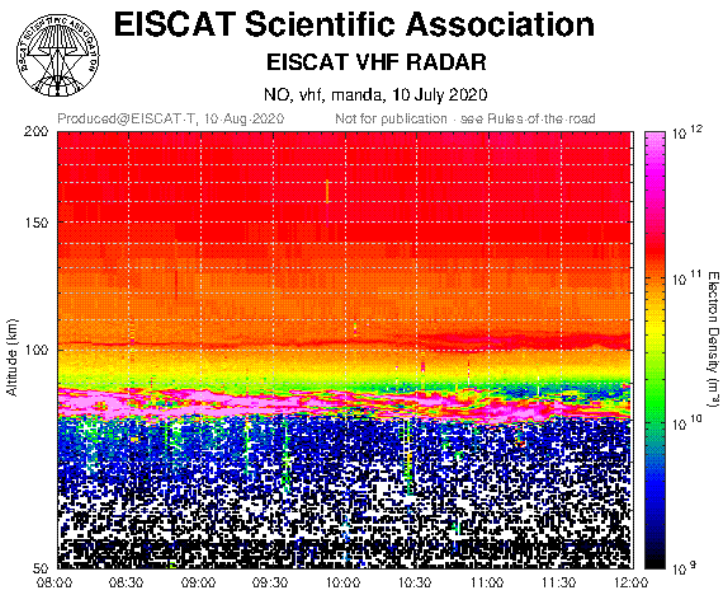

Figure 4.11: PMSE observation 10 July 2020. PMSE is observed as the enhanced EED structure found at altitude range ~80-90 km.

The PMSE spectrum was created the same way as for the PMWE spectrum, described in chapter 3. The resulting plot is seen in figure 4.12. In comparison to the PMWE spectrum seen in figure 3.2 the PMSE spectrum has a peak power of ~65 $\frac{\mathrm{K}}{\mathrm{Hz}}$ being two order of magnitudes larger than the PMWE spectrum's peak power at ~0.10 $\frac{\mathrm{K}}{\mathrm{Hz}}$. It is expected for the PMSE to have a higher peak power since it is known as a stronger mesospheric echo in comparison to PMWE.

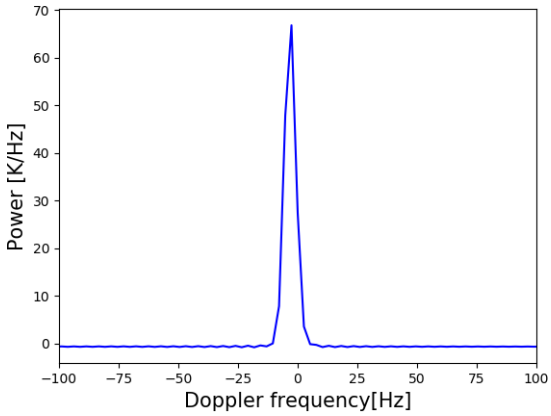

Figure 4.12: PMSE spectrum from PMSE observations 10 July 2020 at altitude 81.28 km and time 10:40 [UT]

When discussing fit of data the results from Strelnikova et al.(2010)[21] was taken into account and it was claimed that PMSE spectrum has a Gaussian distribution due to the echo being coherent. Another possible distribution for the spectrum was Lorentzian, which comes from the ion acoustic dampening occurring at mesospheric region. Since the PMWE spectrum was claimed to be Gaussian given that PMSE spectrum is Gaussian distributed, the best fit for the PMSE spectrum was tested by applying a Gaussian and Lorentzian fit to the spectrum in figure 4.12. Figure 4.13 show the two fittings on the data.

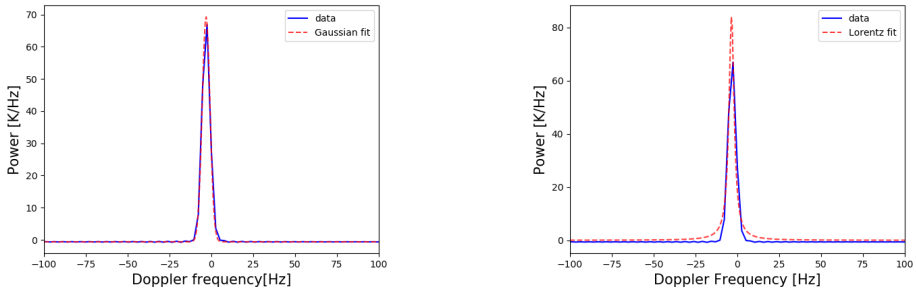

(a) Gaussian fitting **(b)** Lorentzian fitting

Figure 4.13: Gaussian and Lorentzian fitting of data from PMSE observations 10 July 2020 at altitude 81.28 km and time 10:40 [UT]

The Gaussian fit in figure 4.13a follows the shape of the data closely while on the other hand the Lorentzian fit in figure 4.13b shows a peak power higher then the actual data, and also close to the lower power at frequencies +/- 20 Hz it is deviating. This is similar to what we observed for the fitting of PMWE in figure 3.4b. For the PMWE spectrum fitting the Lorentzian deviated at peak

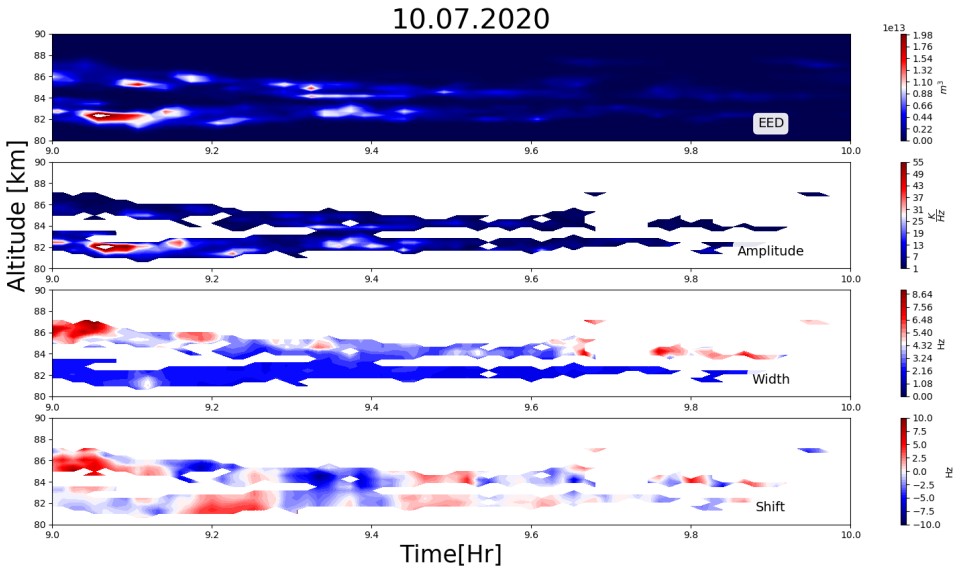

Figure 4.14: PMSE observation 10 July 2020. Time interval for all plots are 09:00-10:00 [UT]. The plots are from top to bottom EED (m^3), amplitude ($\frac{K}{Hz}$), width (Hz) and shift (Hz).

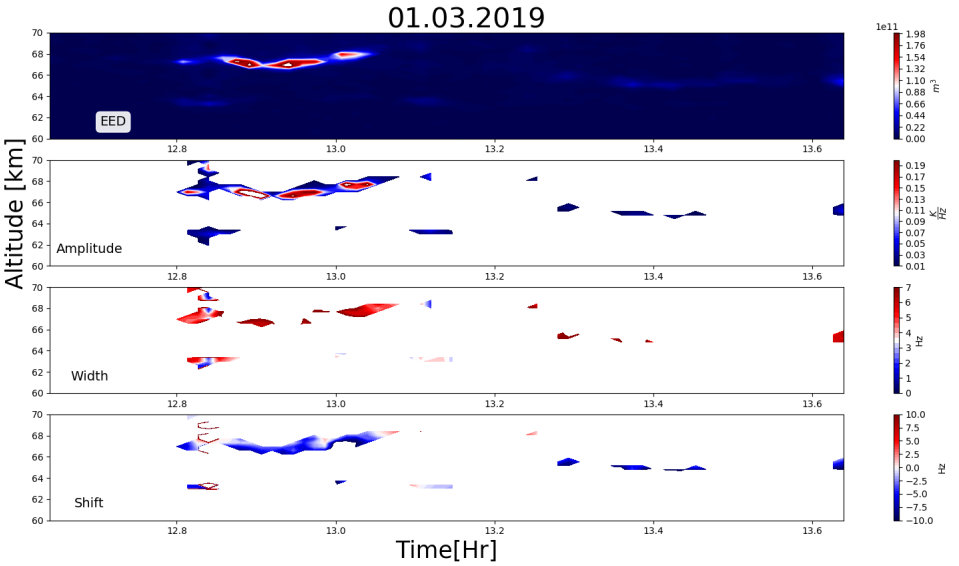

Figure 4.15: PMWE observation 1 March 2019. Figure is also seen in figure **??**, repeated for illustration purposes

power and also close to +/- 20 Hz. The PMSE spectrum is best fitted with a Gaussian distribution and it can be concluded that both mesospheric echoes spectra are best fitted with a Gaussian distribution. Our assumption of PMWE having a Gaussian distribution due to it being a coherent echo like PMSE seems

correct and also justified when looking at the similar behaviours of the two spectra when fitted with the two distributions.

Using the Gaussian fit a figure showing EED and output from Gaussian fitting of the PMSE observation was made, using the same method as for the PMWE observations. The output can be seen in figure 4.14. The goal of the fitting was to look at differences and similarities in the PMSE and PMWE spectra. For comparison the PMWE observation from 1 March 2019 seen in figure 4.15 was chosen since the PMSE observation had no artificial heating occurring simultaneously and the same was desired for the PMWE observation, and the duration of the occurrence was not too short.

Starting with the two top panel in both figure 4.14 and 4.15 the EED values in the PMSE structure is of two orders of magnitude stronger when compared to PMWE. The amplitude for PMSE is also of two orders of magnitude stronger having a peak amplitude of 55 $\frac{K}{Hz}$, while PMWE has a peak value of 0.19 $\frac{K}{Hz}$. PMSE is known as a stronger echo when compared to PMWE[21], which is why higher values in EED and amplitude for PMSE is expected. Moving on to width. PMWE can be observed having an overall width of close to 6 Hz. PMSE in comparison have an overall width in the blue part of the color bar, meaning values close to 3 Hz. An interesting observation is that the observation without artificial heating presented in sub chapter 4.1 (i.e. figure 4.1, 4.2 and 4.3) also have overall width values close to 6 Hz. This could be of interest for further research. It is important to note that only one PMSE case is discussed and that other PMSE observations could provide different width values. Shift values in both figures appears to be similar, neither appearing higher or lower valued. In general for PMWE observations shift has had no deviation in values, staying within the Doppler frequency range -10 - 10 Hz.

Comparing PMWE and PMSE behaviour we can note how both structures seen in EED appears at varying altitudes throughout its occurrence. For PMSE the lowermost structure of the echo at times 9.1 hr is found at an altitude range of ~81-83 km, while at a later time right before 9.4 the same structure is found at an altitude range of ~82-84 km. For PMWE at time close to 12.9 hr the echo is found within the altitude range of ~66-65 km, while later close to 13.1 hr it is found at an altitude range of ~68-69 km. This behaviour could also be of interest for further work on the observations.

5

Conclusion

The goal of this work was to better understand whether dust play a role in the formation of PMWE. This is called the dusty turbulence model, as opposed to the pure turbulence model, which assumes that PMWEs are caused by turbulence without influence of dust.

PMWE observations at 224 MHz identified in the archived data of the EISCAT VHF radar for the years 2008 – 2020 were retrieved and analyzed. The PMWE spectra describing the echo power as a function of frequency were derived and fitting Lorentzian and Gaussian profiles to a selected data set from December 9 2016 observations showed that the spectra are better described with Gaussian profiles. The PMSE, observed on 7 July 2020, considered for comparison were also better described with a Gaussian profile. EISCAT also operates a heating facility that transmits HF radio waves into the ionosphere, increasing the electron temperature. The heater can be operated during radar measurements and is often operated in an on and off sequence, thereby modulating the electron temperature. A total of 11 PMWE observations were evaluated, 4 without simultaneous artificial heating and 7 with.

The amplitudes, widths, and frequency shifts of the PMWE spectra were derived by means of Gaussian fitting. The parameters obtained were presented as a function of the observation time and height of the echo, and the results were discussed. The 4 observations without heating had all an overall spectral

width close to 6 Hz in the PMWE structure. Shift did not wary comparing the artificial heated observations and observations without. A PMSE observation used for comparing PMSE and PMWE also had shift values within the same Doppler frequency range as PMWE (i.e. -10 - 10 Hz).

Among the 7 PMWE observations with artificial heating taking place there were 4 observations with a heating modulation that was suitable for observing overshoots. However, one of them, the 20 February 2014 observation, was excluded due to technical difficulties in the heater operation. From the remaining showed 2 observations (28 February 2012 and 21 November 2014) the characteristics of an overshoot effect indicating that dust played a role in the occurrence of PMWE in these two observations. The author suggests that for these two observations the dusty turbulence theory is the most likely applicable. The last observation with preferable artificial heating modulation, which was 25 January 2012, showed no overshoot effect.

As discussed in this work, the observation of an overshoot can be interpreted due to the influence of dust charging effects on the PMWE, which would support the dusty turbulence model. And this was found for 2 of the observed PMWE. For the other observations we can neither rule out nor confirm that dust is playing a role in forming the observed PMWE. So, it is quite possible that both the pure turbulence model and the dusty turbulence model are applicable.

It is known that PMSEs form in the presence of dust particles. A comparison showed that the PMSE observed on July 10, 2020, had a narrower spectral width in comparison to the March 1 2019 PMWE observation and also in comparison to the 4 cases of PMWE without heating that were considered in this work. For future work, it is proposed to systematically compare the PMWE spectra with the spectra of PMSE. This could help to better understand PMWE as the PMSE process is already better understood.

A

PMWE observations

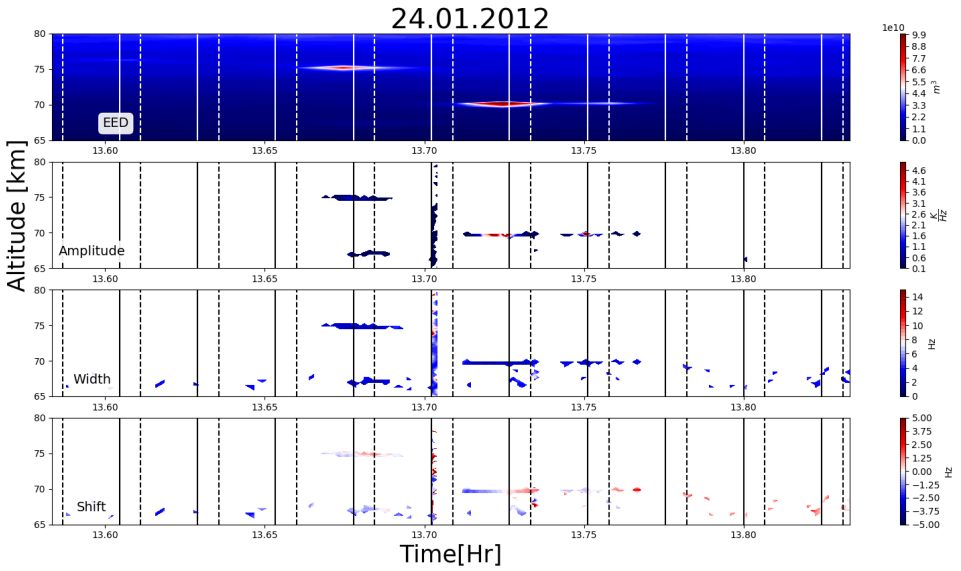

Figure A.1: PMWE observation 24 January 2012. Time interval for all plots are 13:35-13:50 [UT]. The plots are from top to bottom EED (m^3), amplitude ($\frac{K}{Hz}$), width (Hz) and shift (Hz). Continuous white and black lines indicate when heating is turned on and dashed indicates when it was turned off.

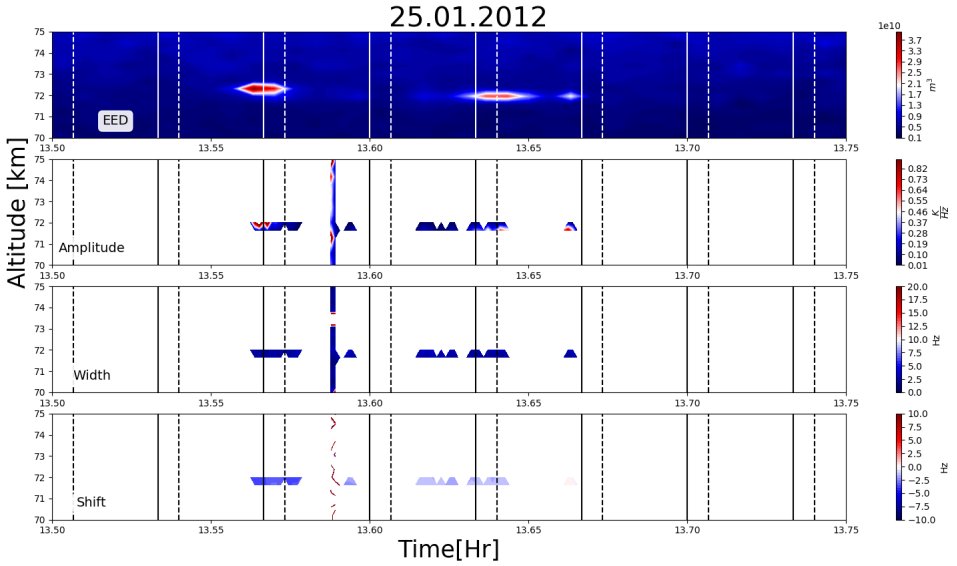

Figure A.2: PMWE observation 25 January 2012. Time interval for all plots are 13:30-13:45 [UT]. The plots are from top to bottom EED (m^3), amplitude ($\frac{K}{Hz}$), width (Hz) and shift (Hz). Continuous white and black lines indicate when heating is turned on and dashed indicates when it was turned off.

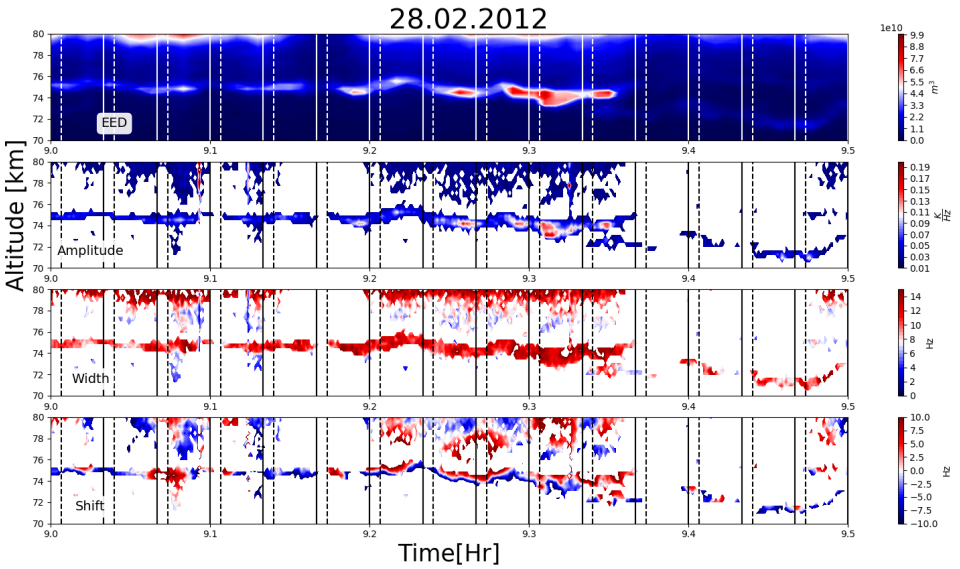

Figure A.3: PMWE observation 28 February 2012. Time interval for all plots are 09:00-09:30 [UT]. The plots are from top to bottom EED (m^3), amplitude ($\frac{K}{Hz}$), width (Hz) and shift (Hz). Continuous white and black lines indicate when heating is turned on and dashed indicates when it was turned off.

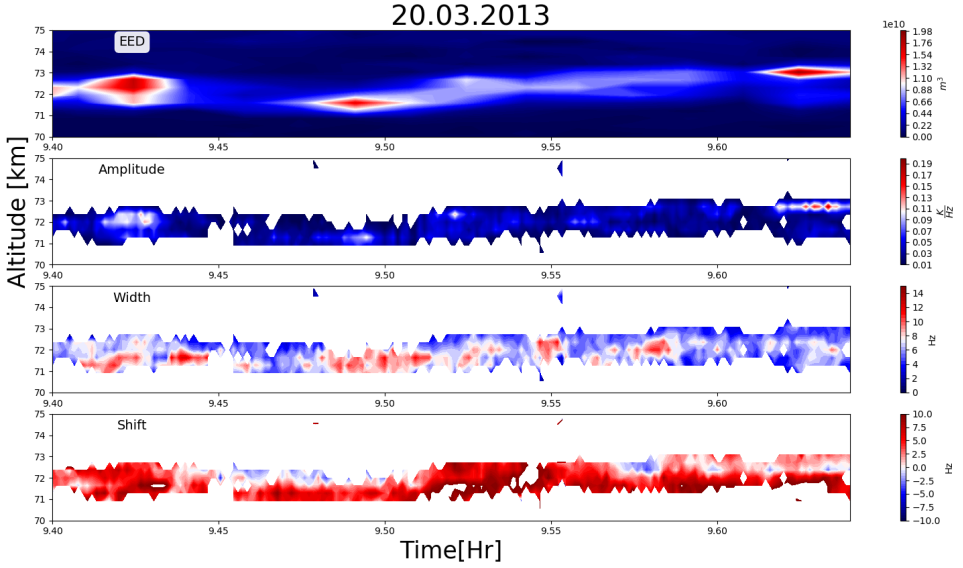

Figure A.4: PMWE observation 20 March 2013. Time interval for all plots are 09:25-09:40 [UT]. The plots are from top to bottom EED (m^3), amplitude ($\frac{K}{Hz}$), width (Hz) and shift (Hz).

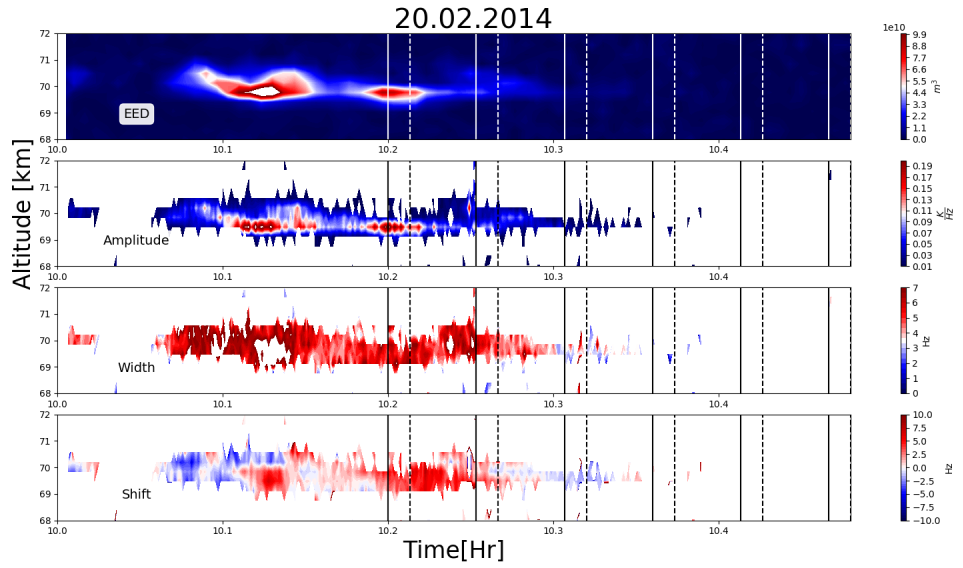

Figure A.5: PMWE observation 20 February 2014. Time interval for all plots are 10:00-10:30 [UT]. The plots are from top to bottom EED (m^3), amplitude ($\frac{K}{Hz}$), width (Hz) and shift (Hz). Continuous white and black lines indicate when heating is turned on and dashed indicates when it was turned off.

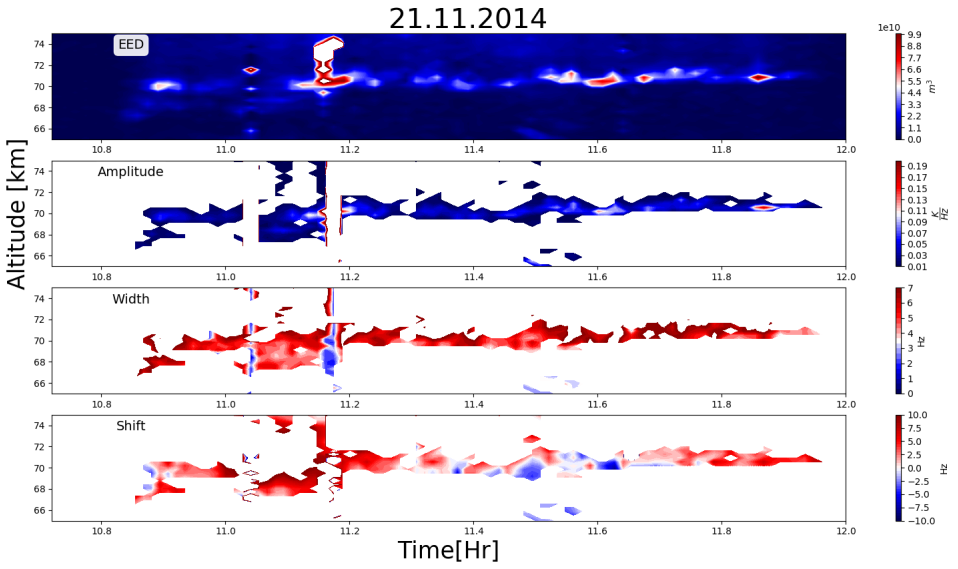

Figure A.6: PMWE observation 21 November 2014. Time interval for all plots are 10:45-12:00 [UT]. The plots are from top to bottom EED (m^3), amplitude ($\frac{K}{Hz}$), width (Hz) and shift (Hz).

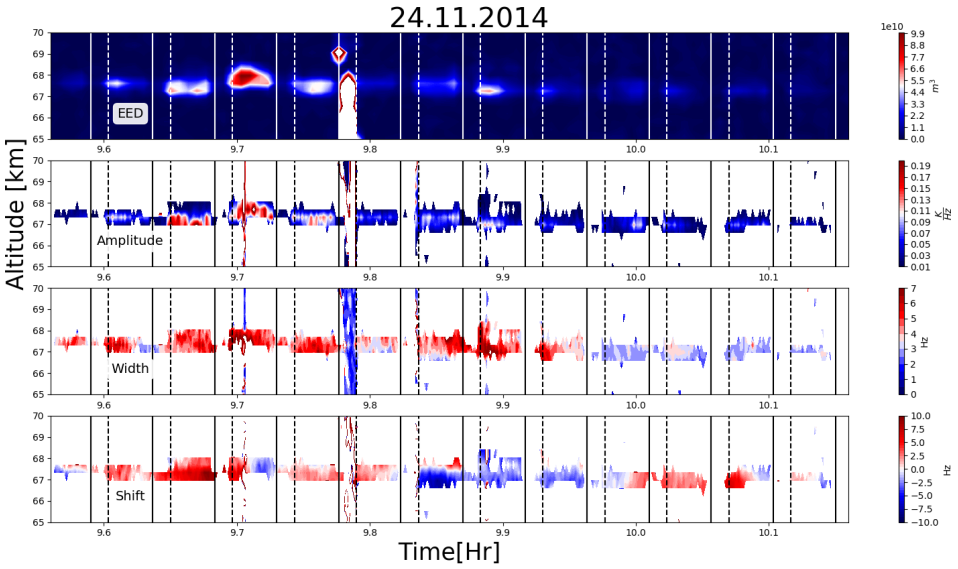

Figure A.7: PMWE observation 24 November 2014. Time interval for all plots are 09:35-10:10 [UT]. The plots are from top to bottom EED (m^3), amplitude ($\frac{K}{Hz}$), width (Hz) and shift (Hz). Continuous white and black lines indicate when heating is turned on and dashed indicates when it was turned off.

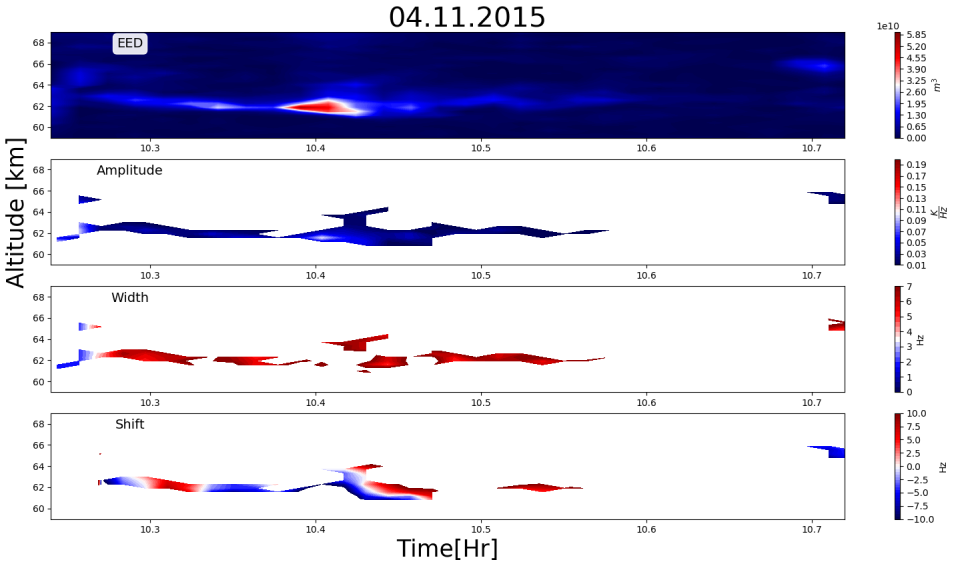

Figure A.8: PMWE observation 4 November 2015. Time interval for all plots are 10:15-10:45 [UT]. The plots are from top to bottom EED (m^3), amplitude ($\frac{K}{Hz}$), width (Hz) and shift (Hz).

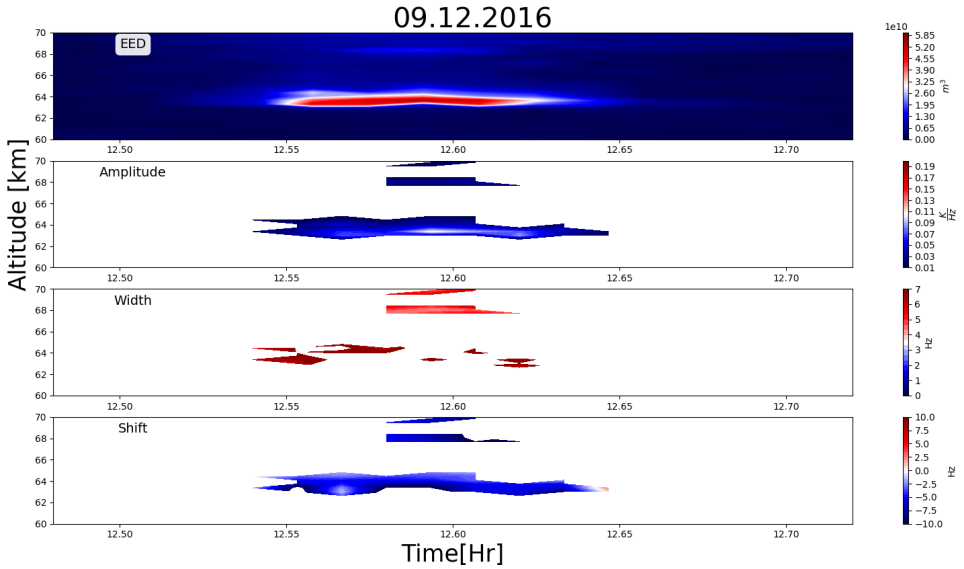

Figure A.9: PMWE observation 9 December 2016. Time interval for all plots are 12:30-12:45 [UT]. The plots are from top to bottom EED (m^3), amplitude ($\frac{K}{Hz}$), width (Hz) and shift (Hz).

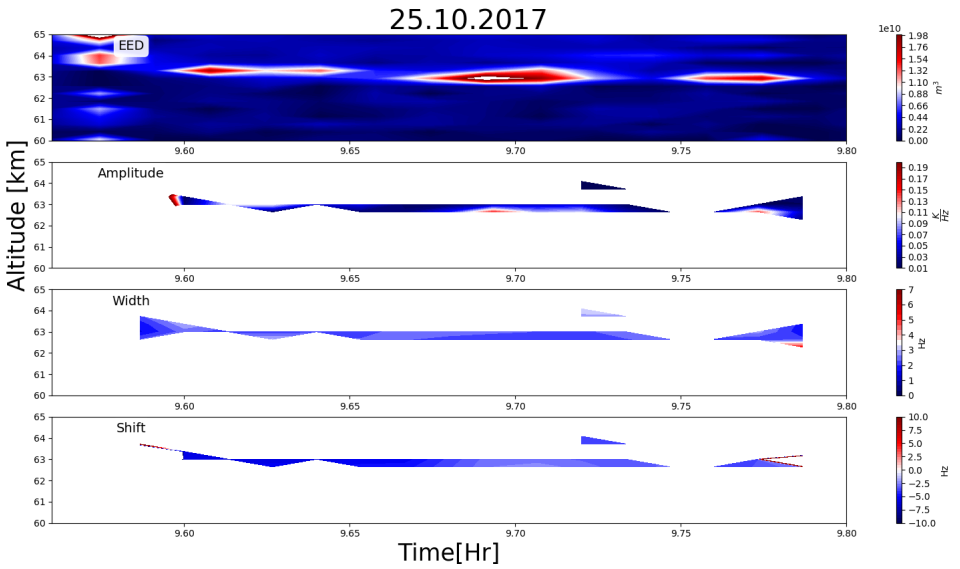

Figure A.10: PMWE observation 25 October 2017. Time interval for all plots are 09:35-09:50 [UT]. The plots are from top to bottom EED (m^3), amplitude ($\frac{K}{Hz}$), width (Hz) and shift (Hz).

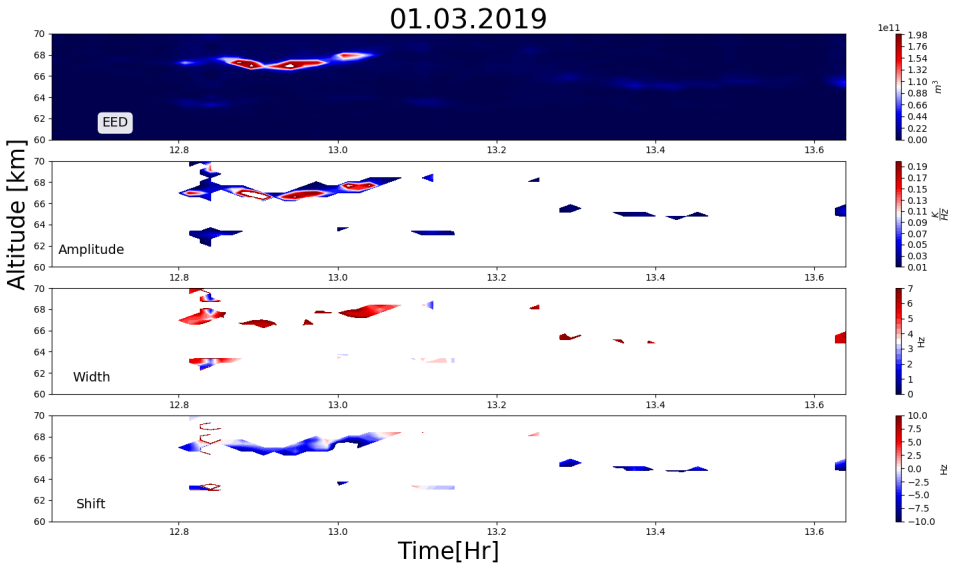

Figure A.11: PMWE observation 1 March 2019. Time interval for all plots are 12:40-13:40 [UT]. The plots are from top to bottom EED (m^3), amplitude ($\frac{K}{Hz}$), width (Hz) and shift (Hz).

/B Code

```
# -*- coding: utf-8 -*-
"""
Created on Wed Mar 30 14:01:42 2022

@author: KristineEttestad
"""

import pandas as pd
import numpy as np
import datetime
import matplotlib.pyplot as plt


#%%
"""
Amplitude, fitwidth, freqpeak and Timevec are all data collected
from running the raw data (collected from EISCAT Portal) in MATLAB
trough Real Time Graph rutine(RTG, https://doi.org/10.5281/zenodo
    .4138625)
in MATLAB.
data is the equivalent electron density collected from madrigal
    database.
"""


Amplitude = np.loadtxt('amplitude.dat', unpack = True)
fitwidth = np.loadtxt('fitwidth.dat', unpack = True)
freqpeak = np.loadtxt('freqpeak.dat', unpack= True)
Timevec = np.loadtxt('Timevec.dat', unpack = True)
data = pd.read_csv('MAD6400_2015-11-04_manda_59.7@vhf.txt', sep=';',
```

```
    header=0)
data.columns = ["YEAR", "MONTH", "DAY", "HOUR","MIN","SEC","RECNO","KINDAT",
                "KINST","UT1_UNIX","UT2_UNIX","AZM","ELM","HSA","POWER",
                "SYSTMP","RANGE","GDAL","NE","TI","TR","CO","VO","PM","PO+",
                "DNE","DTI","DTR","DCO","DVO","DPM","DPO+","DWN","DDC",
                "GFIT","CHISQ"]

#%% Making time and height 1d array

"""
In Timev each column gives a different information of time. The first column
gives year and the last column seconds.
Later when using contourplot only a single 1d time array is needed, therefore
in the next part the three columns cotaining Hour, minute and second is
converted to an array containing hour in decimal format.
"""

Timev = []

hours = Timevec[3]
minutes = Timevec[4]
seconds = Timevec[5]

for i in range(len(hours)):
    t = datetime.time(int(hours[i]),int(minutes[i]),int(seconds[i]))
    ts = (t.hour * 3600 + t.minute * 60 + t.second)/3600
    Timev.append(ts)

"""
Start and end altitude is not given in the data, but based on information
about EISCAT VHF and manda modulated pulse scheme the start heigh is found
about  18 km and ends around 108 km with a resolution of 0.360 km.
Based on this information we create a 1d array for altitude, shown below.
"""

Height = np.arange(18,108,0.360)



#%% Fixing treshold for amplitude

"""
The following line collects the indexs of all Amplitude values foud below
```

```
0.01 K/Hz
"""

row, cols = np.where(Amplitude < 0.01)
#%% Removing noen interesting values from other plots

"""
The values corresponding to the indexes collected from the last cell for
Amplitude, fitwidth and freqpeak is removed and set as empty space.
"""

Amplitude[row,cols]=np.nan

fitwidth[row,cols]=np.nan

freqpeak[row,cols]=np.nan

#%%

"""
This cell is where we work with data collected from madrigal database.

As can be observed in SEC-row, in data, a time step corresponds to 264 rows.
The following 4 lines is how i calculated the lentgh of the time steps.
This methode based on observtaions can be improved.
"""
t_step=792
t_ss = int(t_step/3)
t_0 = int(t_ss)
t_1 = int(t_ss)



"""
Contour plot can be created by either using 1d Array or 2d array(matrix) and
for this data the easiest methode was to create 2d array for altitude,
time and electron density. Firstly we create empty 2d arrays.
"""

A = np.zeros((t_0,int(len(data.MIN)/t_ss)))
Time = np.zeros((t_0,int(len(data.MIN)/t_ss)))
NE = np.zeros((t_0,int(len(data.MIN)/t_ss)))



t=0

""""
```

```
This for-loop creates the time and height 2d arrays. Again using time in hours
in decimal format.
"""

for i in range(int(len(data.MIN)/t_ss)):
    T = data.RANGE[t_ss*i:t_ss*(i+1)]
    y = 0
    for j in T:
        hours = data.HOUR[int(t_ss*i+y)]
        minutes = data.MIN[int(t_ss*i+y)]
        seconds = data.SEC[int(t_ss*i+y)]
        t = datetime.time(hours,minutes,seconds)
        ts = t.hour * 3600 + t.minute * 60 + t.second
        A[y][i] = j
        Time[y][i] = ts/3600
        y += 1

"""
This last for-loop creats the electorn density 2d array
"""

for i in range(int(len(data.MIN)/t_ss)):
        N = data.NE[t_ss*i:t_ss*(i+1)]
        y = 0
        for j in N:
            NE[y][i] = j
            y += 1



#%%

"""
Col         - colormap used when plotting.
y_min,y_max - maximum and minimum altitude of interest
x_min,x_max - start and end time of interest converted to hour(decimal-format)
ranges      - steps on x-axis(time axis)
start       - time when heating starts(decimal-format)
on          - numers of seconds on converted to hours(decimal-format)
off         - numers of seconds off converted to hours(decimal-format)

NB! remove # before start, on and off to include heating with days of hetaing
"""

col = 'seismic'
y_min = 59
y_max = 69

x_min =10+15*1/60+0*1/3600
```

```
168 x_max =10+45*1/60+0*1/3600
169
170 ranges=x_max*10-x_min*10
171 #start = 10 + 2*1/60 + 57*1/3600
172 #on = 48*1/3600
173 #off = 144*1/3600
174
175 """
176 The following section adds all the time when the heater is on and
        off into
177 a 1d array.
178
179 If heating is to be included then simply put # in front of start, on
         and off
180 found in the three lines under this comment.
181 """
182 start= x_max+1
183 on = 0
184 off = 0
185
186 ON = []
187 OFF = []
188 Y = []
189
190 r = 0
191 while start <= x_max:
192     r += 1
193     ON.append(start)
194     start += on
195     OFF.append(start)
196     start += off
197
198
199 print(ON)
200
201 #%%
202
203 """
204 Le is what defines maximum and minimum value of EED, also by
        increasing
205 the last input the numbers of colorlevels are increased.
206 """
207 Le = np.linspace(2e5,6e10,121)
208
209 """
210 Subtitle is the main title placed above all subplots
211 """
212 plt.suptitle('04.11.2015',position=(0.45,0.92),fontsize=30)
213
214 plt.subplot(4,1,1)
215 plt.contourf(Time,A,NE,origin='lower',levels=Le,cmap=col)
216 plt.ylim(y_min,y_max)
217 plt.xlim(x_min,x_max)
218 plt.title("EED", position=(0.10, 0.80),fontsize=14,
```

```
219             bbox=dict(boxstyle="round",color='white',alpha=0.9),
    fontweight=10)
220 """
221 The while loops are where the heating on and off lines are plotted.
222
223 """
224 c = 0
225 while c < r:
226     plt.plot([ON[c],ON[c]],[y_min,y_max],color='white')
227     plt.plot([OFF[c],OFF[c]],[y_min,y_max],color='white',linestyle='
    dashed')
228     c += 1
229
230 plt.colorbar(label='$m^3$')
231 plt.show()
232
233
234 Lev = np.linspace(0.01,0.2,39)
235
236 plt.subplot(4,1,2)
237 plt.contourf(Timev,Height,Amplitude,origin='lower',levels=Lev,cmap=
    col)
238 plt.ylim(y_min,y_max)
239 plt.xlim(x_min,x_max)
240 plt.ylabel('Altitude [km]',fontsize=25)
241 plt.title("Amplitude", position=(0.10,0.80),fontsize=14,
242             bbox=dict(boxstyle="round",color='white',alpha=0.9),
    fontweight=10)
243 c = 0
244 while c < r:
245     plt.plot([ON[c],ON[c]],[y_min,y_max],color='black')
246     plt.plot([OFF[c],OFF[c]],[y_min,y_max],color='black',linestyle='
    dashed')
247     c += 1
248 plt.colorbar(label='$\dfrac{K}{Hz}$')
249 plt.show()
250
251
252 Levv = np.linspace(0,7,22)
253 plt.subplot(4,1,3)
254 plt.contourf(Timev,Height,fitwidth,origin='lower',levels=Levv,cmap=
    col)
255 plt.ylim(y_min,y_max)
256 plt.xlim(x_min,x_max)
257 plt.title("Width", position=(0.10, 0.80),fontsize=14,
258             bbox=dict(boxstyle="round",color='white',alpha=0.9),
    fontweight=10)
259 c = 0
260 while c < r:
261     plt.plot([ON[c],ON[c]],[y_min,y_max],color='black')
262     plt.plot([OFF[c],OFF[c]],[y_min,y_max],color='black',linestyle='
    dashed')
263     c += 1
264 plt.colorbar(label='Hz')
```

```
plt.show()

Levvv = np.linspace(-10,10,41)
plt.subplot(4,1,4)
plt.contourf(Timev,Height,freqpeak,origin='lower',levels=Levvv,cmap=
    col)
plt.ylim(y_min,y_max)
plt.xlim(x_min,x_max)
plt.xlabel('Time[Hr]', fontsize=25)
plt.title("Shift", position=(0.10, 0.80),fontsize=14,
          bbox=dict(boxstyle="round",color='white',alpha=0.9),
    fontweight=10)
c = 0
while c < r:
    plt.plot([ON[c],ON[c]],[y_min,y_max],color='black')
    plt.plot([OFF[c],OFF[c]],[y_min,y_max],color='black',linestyle='
    dashed')
    c += 1
plt.colorbar(label='Hz')
plt.show()
```

Bibliography

[1] E. Belova, Maria Kawnine, Ingemar Häggström, Tima Sergienko, Sheila Kirkwood, and Anders Tjulin. Tristatic observation of polar mesosphere winter echoes with the eiscat vhf radar on 8 january 2014: a case study. Earth, Planets and Space, 70, 12 2018.

[2] A. Biebricher, O. Havnes, T.W. Hartquist, and C. LaHoz. On the influence of plasma absorption by dust on the pmse overshoot effect. Advances in Space Research, 38(11):2541–2550, 2006. Middle and Upper Atmospheres, Active Experiments, and Dusty Plasmas.

[3] H. Flohn and R. Penndorf. The stratification of the atmosphere (i). Bulletin of the American Meteorological Society, 31(3):71 – 78, 1950.

[4] O. Havnes, C. La Hoz, A. Aylward, E. Belova, T.W. Hartquist, M.J. Kosch, G. Morfill, G.O.L. Jones, L.I. Næsheim, M.T. Rietveld, M. Rubin-Zuzic, and F. Sigernes. Observations of the overshoot effect during the 2004 eiscat pmse campaign. Advances in Space Research, 38(11):2344–2352, 2006. Middle and Upper Atmospheres, Active Experiments, and Dusty Plasmas.

[5] Ove Havnes, Torsten Aslaksen, and Alvin Brattli. Charged dust in the earth's middle atmosphere. Physica Scripta, T89(1):133, 2001.

[6] Varun Jain, Mark C. Biesinger, and Matthew R. Linford. The gaussian-lorentzian sum, product, and convolution (voigt) functions in the context of peak fitting x-ray photoelectron spectroscopy (xps) narrow scans. Applied Surface Science, 447:548–553, 2018.

[7] M. Kassa, O. Havnes, and E. Belova. The effect of electron bite-outs on artificial electron heating and the pmse overshoot. Annales Geophysicae, 23(12):3633–3643, 2005.

[8] Sheila Kirkwood. Polar mesosphere winter echoes – a review of recent results. Advances in Space Research, 40:751–757, 12 2007.

[9] C. La Hoz and O. Havnes. Artificial modification of polar mesospheric winter echoes with an RF heater: Do charged dust particles play an active role? Journal of Geophysical Research (Atmospheres), 113(D19):D19205, October 2008.

[10] R. Latteck and I. Strelnikova. Extended observations of polar mesosphere winter echoes over Andøya (69°N) using MAARSY. Journal of geophysical research, 120, 2015.

[11] Franz-Josef Lübken, Martin J. Jarvis, and G. Owen L. Jones. First in situ temperature measurements at the antarctic summer mesopause. Geophysical Research Letters, 26(24):3581–3584, 1999.

[12] Viswanathan Lakshmi Narayanan, Ingemar Häggström, and Ingrid Mann. Effects of particle precipitation on the polar mesospheric summer echoes observed by eiscat vhf 224 mhz radar. Advances in Space Research, 69(9):3350–3361, 2022.

[13] Toralf Renkwitz Ralph Latteck and Jorge L. Chau. Two decades of long-term observations of polar mesospheric echoes at 69°N. Journal of Atmospheric and Solar-Terretrsial Physics, 216, 2021.

[14] M Rapp and Lübken F.-J. Polar mesosphere summer echoes (pmse): Review of observations and current understanding. Atmospheric Chemistry and Physics Discussions, 4, 12 2004.

[15] M. Rapp, F.-J. Lübken, and T. A. Blix. Small scale density variations of electrons and charged particles in the vicinity of polar mesosphere summer echoes. Atmospheric Chemistry and Physics, 3(5):1399–1407, 2003.

[16] Markus Rapp, Irina Strelnikova, and Jörg Gumbel. Meteoric smoke particles: Evidence from rocket and radar techniques. Advances in Space Research, 40(6):809–817, 2007.

[17] Markus Rapp, Irina Strelnikova, Ralph Latteck, Peter Hoffmann, Ulf-Peter Hoppe, Ingemar Häggström, and Michael T. Rietveld. Polar mesosphere summer echoes (pmse) studied at bragg wavelengths of 2.8m, 67cm, and 16cm. Journal of Atmospheric and Solar-Terrestrial Physics, 70(7):947–961, 2008.

[18] M.T Rietveld, H Kohl, H Kopka, and P Stubbe. Introduction to ionospheric heating at tromsø—i. experimental overview. Journal of Atmospheric and Terrestrial Physics, 55(4):577–599, 1993. The Fifth International EISCAT

Workshop.

[19] H. Rishbeth. The ionospheric e-layer and f-layer dynamos — a tutorial review. Journal of Atmospheric and Solar-Terrestrial Physics, 59(15):1873–1880, 1997.

[20] Boris Strelnikov, Tristan Staszak, Ralph Latteck, Toralf Renkwitz, Irina Strelnikova, Franz-Josef Lübken, Gerd Baumgarten, Jens Fiedler, Jorge L. Chau, Joan Stude, Markus Rapp, Martin Friedrich, Jörg Gumbel, Jonas Hedin, Evgenia Belova, Marcus Hörschgen-Eggers, Gabriel Giono, Igor Hörner, Stefan Löhle, Martin Eberhart, and Stefanos Fasoulas. Sounding rocket project "pmwe" for investigation of polar mesosphere winter echoes. Journal of Atmospheric and Solar-Terrestrial Physics, 218:105596, 2021.

[21] Irina Strelnikova and Markus Rapp. Studies of polar mesosphere summer echoes with the eiscat vhf and uhf radars: Information contained in the spectral shape. Advances in Space Research, 45(2):247–259, 2010.

[22] Irina Strelnikova, Markus Rapp, Shikha Raizada, and Mike Sulzer. Meteor smoke particle properties derived from arecibo incoherent scatter radar observations. Geophysical Research Letters, 34, 08 2007.

[23] Tsuda T. Characteristics of atmospheric gravity waves observed using the mu (middle and upper atmosphere) radar and gps (global positioning system) radio occultation. Physical and biological sciences, 90(1):12–27, 2014.

[24] Anders Tjulin. EISCAT experiments. `https://www.eiscat.se/wp-content/uploads/2017/04/Experiments.pdf`, 2017. Accessed: 07 Dec, 2021.

[25] T. Turunen, A. Westman, I. Häggström, and G. Wannberg. High resolution general purpose d-layer experiment for eiscat incoherent scatter radars using selected set of random codes. Annales Geophysicae, 20(9):1469–1477, 2002.